themselves, substantially influence the efficiency of duplex DNA formation in each hepatocyte, at the level of post-vector entry processing of rAAV vectors. In other words, in rAAV2-nonpermissive hepatocytes, which account for ≈90% of total hepatocytes and can take up rAAV2 vectors but not express transgene product, duplex rAAV2 vector genome formation is impaired at the level of post-vector entry when vector genomes are delivered with AAV2 capsids but not impaired when they are delivered with AAV8 capsids.

The tissue biodistibution profile after systemic administration of the rAAV8 vector has been reported in a study with a hemophilia A mouse model (49). They injected mice with 10^{10} to 10^{11} vg of canine coagulation factor VIII-expressing vector and quantified vector genome copy numbers by TaqMan PCR. They concluded that rAAV8 has strong tropism to the liver, but no apparent vector genome dissemination was observed, although they found 0.26 to 0.70 copy/cell signals in the hearts of 2 out of 21 mice examined and 0.41 to 0.77 copy/cell signals in the lungs of 3 out of 21 animals examined, the significance of which was not discussed in their report. It should be noted that these two organs are among the four organs that had vector genomes at levels over 10 ds-vg/dge in our study.

In our study, we have clearly demonstrated that, in the context of the cytomegalovirus promoter, rAAV8 transduced the heart with an extremely high efficiency even at a dose of 3.0×10^{11} vg/mouse, and the heart was the best-transduced tissue among all the tissues analyzed including the liver at 3.0×10^{11} vg/mouse. At a dose of 7.2×10^{12} vg/mouse, 100% of cardiomyocytes were transduced. Although we could not determine the minimum rAAV8 vector dose required for 100% cardiomyocyte transduction, it is presumed to be much less than 7.2×10^{12} vg/mouse, given that 3.0×10^{11} vg/mouse was sufficient to transduce a majority of cardiomyocytes. Skeletal muscles were also well transduced at a high vector dose. At a dose of 7.2×10^{12} vg/mouse, virtually all the myofibers in the entire skeletal muscle system throughout the body were transduced, although they were less susceptible to rAAV8 than cardiac muscle, given that not many myofibers were transduced at a dose of 3.0×10^{11} vg/mouse. Recently, Gregorevic et al. have shown that intravascular administration of rAAV6 vectors resulted in widespread skeletal muscle transduction and entire cardiac muscle transduction, as we have observed with rAAV8 in our present study, and they also have established proof of principle that systemic administration of a rAAV6 vector can be used to treat Duchenne muscular dystrophy (16). It should be noted that, in order to increase the permeability of the peripheral microvasculature, their method required simultaneous injection of vascular endothelium growth factor, which was not needed in the context of the rAAV8 vectors.

It is also intriguing that we observed extensive transduction in the pancreas with rAAV8 without any histological evidence suggestive of cell damage or inflammation. In agreement with the previous report on rAAV8 (55), pancreatic acinar cells were the major target, but insulin-producing pancreatic islet cells were also transduced to a certain extent. Our study has demonstrated that systemic administration of rAAV8 vectors could achieve pancreatic transduction at levels equivalent to or even higher than that achievable with adenovirus vectors (55).

It was surprising to us that tail vein or portal vein injection of the rAAV8 vector could transduce broad regions of the brain, since in general it is not possible to transduce this organ by systemic intravenous administration of viral vectors due to the presence of the blood-brain barrier. rAAV vector shedding with negligible levels in the brain has occasionally been reported in tissue distribution preclinical studies (10, 17, 32, 49, 58). However, none of these studies have investigated the origins of the PCR-positive signals. Whether rAAV traversed the blood-brain barrier and transduced neurons and glial cells or remained in the connective tissues including blood vessels has not been addressed. It is intriguing that the median eminence and arcuate nucleus of the hypothalamus and basolateral nucleus of the amygdala were focally transduced with high efficiency. The mechanism(s) underlying focal high transduction is not clear but may be related to a rich blood supply. Interestingly, the hypothalamus is known to have fenestrated capillaries that have numerous small pores increasing vascular permeability.

Dissemination of the viral vectors to the brain is a serious concern in terms of liver gene therapy, but gene delivery to neurons and glial cells by viral vectors holds great promise for gene therapy for central nervous system diseases. Direct intracranial injection of vectors allows efficient transduction of brain tissue, but the transduction is normally limited to the vicinity of the injection site. Many central nervous system diseases broadly affect brain tissue, and therefore global brain transduction by alternative approaches is often preferred. However, the presence of the blood-brain barrier has precluded widespread transduction of the brain. Recently, two strategies, in utero gene transfer (26, 27) and systemic or regional viral administration after mannitol infusion (13, 28), have been shown to successfully overcome this hurdle. The former approach takes advantage of the immaturity of the fetus's blood-brain barrier with increased permeability, and the latter transiently disrupts the blood-brain barrier by making a hyperosmotic environment in the brain capillaries. The mechanisms by which rAAV8 could efficiently traverse the intact blood-brain barrier have yet to be elucidated, and whether rAAV8 particles were actively escorted by a not-yet-defined system or the high dose of rAAV8 vector infusion itself damaged the blood-brain barrier needs to be addressed.

It should be noted that the viral preparation we used for this study contained 5% sorbitol in PBS. Sorbitol is a carbohydrate with the same molecular weight as mannitol and is used clinically to introduce a hyperosmotic environment. Fu et al. reported that, in order to open the blood-brain barrier and transduce mouse brain tissue with intravenously administered rAAV2, preinfusion of 200 μl of 25% mannitol (corresponding to 50 mg of mannitol) was required, and simultaneous infusion of the same amount of 12.5% mannitol (corresponding to 25 mg) had no effect. In our study, we injected 300 μl of vector preparations (equivalent to 15 mg of mannitol), and therefore it is unlikely that our excipient contributed to the transient disruption of the blood-brain barrier. Nonetheless, our study clearly demonstrated that intravenous administration of rAAV8 vectors can transduce neurons and glial cells in broad regions of the adult mouse brain without any treatment that disrupts the blood-brain barrier. Although the mechanism is not clear, rAAV8 will offer an alternative approach to global central nervous system gene delivery in combination with currently available strategies.

Except for the liver, direct injection into the target tissue is a standard approach for transduction with rAAV vectors. This approach is desirable because it can minimize the possibility of vector dissemination to remote organs. However, it has often suffered from the confinement of vectors to the injection site, precluding widespread transduction in a target organ. In this regard, rAAV8 may be applied for global transduction in a given nonhepatic target organ. All the tissues analyzed had double-stranded rAAV8 vector genomes at levels of at least 2 ds-vg/dge. It is important to emphasize that vector dissemination was determined by genomic DNA Southern blot analysis and not a PCR-based assay. This method is superior in detecting double-stranded vector genomes formed within cells. It should be noted that transduction efficiency determined by transgene expression and vector genome copy numbers were not correlated. Presumably the promoter activities vary among the tissues, and it is possible that the tissues with a limited number of β-galactosidase-positive cells in the context of the EF1α or cytomegalovirus enhancer-promoter would have substantial transduction if a different enhancer-promoter is used. Further investigation will be needed to address these discrepancies.

In summary, we demonstrate that all hepatocytes are able to convert incoming single-stranded vector genomes to duplex DNA and are permissive to stable transduction with rAAV8 vectors. In contrast to rAAV2 vectors, ≈100% hepatocyte transduction with the rAAV8 vector could be achieved, and multiple organs could be transduced with extremely high efficiencies following a peripheral vein injection simply by increasing the vector dose. These results not only provide new insights into the mechanisms of liver transduction with rAAV vectors but also open up new applications for rAAV8 vectors in gene therapy, functional genomics, and generating various disease animal models, although, from a safety point of view, a high-dose systemic rAAV8 vector injection strategy will need to take into account the promiscuous tropism of this vector.

ACKNOWLEDGMENTS

We thank Makoto Yamakado for histological analysis.

This work was supported by a National Hemophilia Foundation Career Development Award to H.N. and an NIH grant HL66948 to M.A.K.

REFERENCES

1. **Alexander, I. E., D. W. Russell, and A. D. Miller.** 1994. DNA-damaging agents greatly increase the transduction of nondividing cells by adeno-associated virus vectors. J. Virol. **68**:8282–8287.
2. **Alexander, I. E., D. W. Russell, A. M. Spence, and A. D. Miller.** 1996. Effects of gamma irradiation on the transduction of dividing and nondividing cells in brain and muscle of rats by adeno-associated virus vectors. Hum. Gene Ther. **7**:841–850.
3. **Burton, M., H. Nakai, P. Colosi, J. Cunningham, R. Mitchell, and L. Couto.** 1999. Coexpression of factor VIII heavy and light chain adeno-associated viral vectors produces biologically active protein. Proc. Natl. Acad. Sci. USA **96**:12725–12730.
4. **Chao, H., Y. Liu, J. Rabinowitz, C. Li, R. J. Samulski, and C. E. Walsh.** 2000. Several log increase in therapeutic transgene delivery by distinct adeno-associated viral serotype vectors. Mol. Ther. **2**:619–623.
5. **Chen, S. J., J. Tazelaar, and J. M. Wilson.** 2001. Selective repopulation of normal mouse liver by hepatocytes transduced in vivo with recombinant adeno-associated virus. Hum. Gene Ther. **12**:45–50.
6. **Chiorini, J. A., L. Yang, Y. Liu, B. Safer, and R. M. Kotin.** 1997. Cloning of adeno-associated virus type 4 (AAV4) and generation of recombinant AAV4 particles. J. Virol. **71**:6823–6833.
7. **Davidson, B. L., C. S. Stein, J. A. Heth, I. Martins, R. M. Kotin, T. A. Derksen, J. Zabner, A. Ghodsi, and J. A. Chiorini.** 2000. Recombinant adeno-associated virus type 2, 4, and 5 vectors: transduction of variant cell types and regions in the mammalian central nervous system. Proc. Natl. Acad. Sci. USA **97**:3428–3432.
8. **Duan, D., P. Sharma, J. Yang, Y. Yue, L. Dudus, Y. Zhang, K. J. Fisher, and J. F. Engelhardt.** 1998. Circular intermediates of recombinant adeno-associated virus have defined structural characteristics responsible for long-term episomal persistence in muscle tissue. J. Virol. **72**:8568–8577.
9. **Duan, D., Y. Yue, Z. Yan, J. Yang, and J. F. Engelhardt.** 2000. Endosomal processing limits gene transfer to polarized airway epithelia by adeno-associated virus. J. Clin. Investig. **105**:1573–1587.
10. **Favre, D., N. Provost, V. Blouin, G. Blancho, Y. Cherel, A. Salvetti, and P. Moullier.** 2001. Immediate and long-term safety of recombinant adeno-associated virus injection into the nonhuman primate muscle. Mol. Ther. **4**:559–566.
11. **Ferrari, F. K., T. Samulski, T. Shenk, and R. J. Samulski.** 1996. Second-strand synthesis is a rate-limiting step for efficient transduction by recombinant adeno-associated virus vectors. J. Virol. **70**:3227–3234.
12. **Fisher, K. J., G. P. Gao, M. D. Weitzman, R. DeMatteo, J. F. Burda, and J. M. Wilson.** 1996. Transduction with recombinant adeno-associated virus for gene therapy is limited by leading-strand synthesis. J. Virol. **70**:520–532.
13. **Fu, H., J. Muenzer, R. J. Samulski, G. Breese, J. Sifford, X. Zeng, and D. M. McCarty.** 2003. Self-complementary adeno-associated virus serotype 2 vector: global distribution and broad dispersion of AAV-mediated transgene expression in mouse brain. Mol. Ther. **8**:911–917.
14. **Gao, G., L. H. Vandenberghe, M. R. Alvira, Y. Lu, R. Calcedo, X. Zhou, and J. M. Wilson.** 2004. Clades of Adeno-associated viruses are widely disseminated in human tissues. J. Virol. **78**:6381–6388.
15. **Gao, G. P., M. R. Alvira, L. Wang, R. Calcedo, J. Johnston, and J. M. Wilson.** 2002. Novel adeno-associated viruses from rhesus monkeys as vectors for human gene therapy. Proc. Natl. Acad. Sci. USA **99**:11854–11859.
16. **Gregorevic, P., M. J. Blankinship, J. M. Allen, R. W. Crawford, L. Meuse, D. G. Miller, D. W. Russell, and J. S. Chamberlain.** 2004. Systemic delivery of genes to striated muscles using adeno-associated viral vectors. Nat. Med. **10**:828–834.
17. **Grimm, D., S. Zhou, H. Nakai, C. E. Thomas, T. A. Storm, S. Fuess, T. Matsushita, J. Allen, R. Surosky, M. Lochrie, L. Meuse, A. McClelland, P. Colosi, and M. A. Kay.** 2003. Preclinical in vivo evaluation of pseudotyped adeno-associated virus vectors for liver gene therapy. Blood **102**:2412–2419.
18. **Hanaoka, K., M. Hayasaka, T. Uetsuki, A. Fujisawa-Sehara, and Y. Nabeshima.** 1991. A stable cellular marker for the analysis of mouse chimeras: the bacterial chloramphenicol acetyltransferase gene driven by the human elongation factor 1α promoter. Differentiation. **48**:183–189.
19. **Hansen, J., K. Qing, and A. Srivastava.** 2001. Adeno-associated virus type 2-mediated gene transfer: altered endocytic processing enhances transduction efficiency in murine fibroblasts. J. Virol. **75**:4080–4090.
20. **Kaemmerer, W. F., R. G. Reddy, C. A. Warlick, S. D. Hartung, R. S. McIvor, and W. C. Low.** 2000. In vivo transduction of cerebellar Purkinje cells using adeno-associated virus vectors. Mol. Ther. **2**:446–457.
21. **Kay, M. A., Q. Li, T. J. Liu, F. Leland, C. Toman, M. Finegold, and S. L. Woo.** 1992. Hepatic gene therapy: persistent expression of human α1-antitrypsin in mice after direct gene delivery in vivo. Hum. Gene Ther. **3**:641–647.
22. **Kay, M. A., C. S. Manno, M. V. Ragni, P. J. Larson, L. B. Couto, A. McClelland, B. Glader, A. J. Chew, S. J. Tai, R. W. Herzog, V. Arruda, F. Johnson, C. Scallan, E. Skarsgard, A. W. Flake, and K. A. High.** 2000. Evidence for gene transfer and expression of factor IX in haemophilia B patients treated with an AAV vector. Nat. Genet. **24**:257–261.
23. **Kessler, P. D., G. M. Podsakoff, X. Chen, S. A. McQuiston, P. C. Colosi, L. A. Matelis, G. J. Kurtzman, and B. J. Byrne.** 1996. Gene delivery to skeletal muscle results in sustained expression and systemic delivery of a therapeutic protein. Proc. Natl. Acad. Sci. USA **93**:14082–14087.
24. **Kim, I. H., A. Jozkowicz, P. A. Piedra, K. Oka, and L. Chan.** 2001. Lifetime correction of genetic deficiency in mice with a single injection of helper-dependent adenoviral vector. Proc. Natl. Acad. Sci. USA **98**:13282–13287.
25. **Kojima, H., M. Fujimiya, K. Matsumura, P. Younan, H. Imaeda, M. Maeda, and L. Chan.** 2003. Neuro-D-betacellulin gene therapy induces islet neogenesis in the liver and reverses diabetes in mice. Nat. Med. **9**:596–603.
26. **Lai, L., B. B. Davison, R. S. Veazey, K. J. Fisher, and G. B. Baskin.** 2002. A preliminary evaluation of recombinant adeno-associated virus biodistribution in rhesus monkeys after intrahepatic inoculation in utero. Hum. Gene Ther. **13**:2027–2039.
27. **Lipshutz, G. S., D. Titre, M. Brindle, A. R. Bisconte, C. H. Contag, and K. M. Gaensler.** 2003. Comparison of gene expression after intraperitoneal delivery of AAV2 or AAV5 in utero. Mol. Ther. **8**:90–98.
28. **Mastakov, M. Y., K. Baer, R. Xu, H. Fitzsimons, and M. J. During.** 2001. Combined injection of rAAV with mannitol enhances gene expression in the rat brain. Mol. Ther. **3**:225–232.
29. **McCaffrey, A. P., H. Nakai, K. Pandey, Z. Huang, F. H. Salazar, H. Xu, S. F. Wieland, P. L. Marion, and M. A. Kay.** 2003. Inhibition of hepatitis B virus in mice by RNA interference. Nat. Biotechnol. **21**:639–644.
30. **McCarty, D. M., H. Fu, P. E. Monahan, C. E. Toulson, P. Naik, and R. J. Samulski.** 2003. Adeno-associated virus terminal repeat (TR) mutant gen-

erates self-complementary vectors to overcome the rate-limiting step to transduction in vivo. Gene Ther. 10:2112–2118.
31. **McCarty, D. M., P. E. Monahan, and R. J. Samulski.** 2001. Self-complementary recombinant adeno-associated virus (scAAV) vectors promote efficient transduction independently of DNA synthesis. Gene Ther. 8:1248–1254.
32. **Miao, C. H., H. Nakai, A. R. Thompson, T. A. Storm, W. Chiu, R. O. Snyder, and M. A. Kay.** 2000. Nonrandom transduction of recombinant adeno-associated virus vectors in mouse hepatocytes in vivo: cell cycling does not influence hepatocyte transduction. J. Virol. 74:3793–3803.
33. **Miao, C. H., R. O. Snyder, D. B. Schowalter, G. A. Patijn, B. Donahue, B. Winther, and M. A. Kay.** 1998. The kinetics of rAAV integration in the liver. Nat. Genet. 19:13–15.
34. **Nakai, H., R. W. Herzog, J. N. Hagstrom, J. Walter, S. H. Kung, E. Y. Yang, S. J. Tai, Y. Iwaki, G. J. Kurtzman, K. J. Fisher, P. Colosi, L. B. Couto, and K. A. High.** 1998. Adeno-associated viral vector-mediated gene transfer of human blood coagulation factor IX into mouse liver. Blood 91:4600–4607.
35. **Nakai, H., Y. Iwaki, M. A. Kay, and L. B. Couto.** 1999. Isolation of recombinant adeno-associated virus vector-cellular DNA junctions from mouse liver. J. Virol. 73:5438–5447.
36. **Nakai, H., T. A. Storm, S. Fuess, and M. A. Kay.** 2003. Pathways of removal of free DNA vector ends in normal and DNA-PKcs-deficient SCID mouse hepatocytes transduced with rAAV vectors. Hum. Gene Ther. 14:871–881.
37. **Nakai, H., T. A. Storm, and M. A. Kay.** 2000. Increasing the size of rAAV-mediated expression cassettes in vivo by intermolecular joining of two complementary vectors. Nat. Biotechnol. 18:527–532.
38. **Nakai, H., T. A. Storm, and M. A. Kay.** 2000. Recruitment of single-stranded recombinant adeno-associated virus vector genomes and intermolecular recombination are responsible for stable transduction of liver in vivo. J. Virol. 74:9451–9463.
39. **Nakai, H., C. E. Thomas, T. A. Storm, S. Fuess, S. Powell, W. J. F., and M. A. Kay.** 2002. A limited number of transducible hepatocytes restricts a wide-range linear vector dose response in rAAV-mediated liver transduction. J. Virol. 76:11343–11349.
40. **Nakai, H., S. R. Yant, T. A. Storm, S. Fuess, L. Meuse, and M. A. Kay.** 2001. Extrachromosomal recombinant adeno-associated virus vector genomes are primarily responsible for stable liver transduction in vivo. J. Virol. 75:6969–6976.
41. **Overturf, K., M. Al-Dhalimy, R. Tanguay, M. Brantly, C. N. Ou, M. Finegold, and M. Grompe.** 1996. Hepatocytes corrected by gene therapy are selected in vivo in a murine model of hereditary tyrosinaemia type I. Nat. Genet. 12:266–273.
42. **Ponder, K. P., J. R. Melniczek, L. Xu, M. A. Weil, T. M. O'Malley, P. A. O'Donnell, V. W. Knox, G. D. Aguirre, H. Mazrier, N. M. Ellinwood, M. Sleeper, A. M. Maguire, S. W. Volk, R. L. Mango, J. Zweigle, J. H. Wolfe, and M. E. Haskins.** 2002. Therapeutic neonatal hepatic gene therapy in mucopolysaccharidosis VII dogs. Proc. Natl. Acad. Sci. USA 99:13102–13107.
43. **Qing, K., J. Hansen, K. A. Weigel-Kelley, M. Tan, S. Zhou, and A. Srivastava.** 2001. Adeno-associated virus type 2-mediated gene transfer: role of cellular FKBP52 protein in transgene expression. J. Virol. 75:8968–8976.
44. **Qing, K., W. Li, L. Zhong, M. Tan, J. Hansen, K. A. Weigel-Kelley, L. Chen, M. C. Yoder, and A. Srivastava.** 2003. Adeno-associated virus type 2-mediated gene transfer: role of cellular T-cell protein tyrosine phosphatase in transgene expression in established cell lines in vitro and transgenic mice in vivo. J. Virol. 77:2741–2746.
45. **Qing, K., X. S. Wang, D. M. Kube, S. Ponnazhagan, A. Bajpai, and A. Srivastava.** 1997. Role of tyrosine phosphorylation of a cellular protein in adeno-associated virus 2-mediated transgene expression. Proc. Natl. Acad. Sci. USA 94:10879–10884.
46. **Rabinowitz, J. E., F. Rolling, C. Li, H. Conrath, W. Xiao, X. Xiao, and R. J. Samulski.** 2002. Cross-packaging of a single adeno-associated virus (AAV) type 2 vector genome into multiple AAV serotypes enables transduction with broad specificity. J. Virol. 76:791–801.
47. **Rutledge, E. A., C. L. Halbert, and D. W. Russell.** 1998. Infectious clones and vectors derived from adeno-associated virus (AAV) serotypes other than AAV type 2. J. Virol. 72:309–319.
48. **Sanlioglu, S., P. K. Benson, J. Yang, E. M. Atkinson, T. Reynolds, and J. F. Engelhardt.** 2000. Endocytosis and nuclear trafficking of adeno-associated virus type 2 are controlled by rac1 and phosphatidylinositol-3 kinase activation. J. Virol. 74:9184–9196.
49. **Sarkar, R., R. Tetreault, G. Gao, L. Wang, P. Bell, R. Chandler, J. M. Wilson, and H. H. Kazazian, Jr.** 2004. Total correction of hemophilia A mice with canine FVIII using an AAV 8 serotype. Blood 103:1253–1260.
50. **Seisenberger, G., M. U. Ried, T. Endress, H. Buning, M. Hallek, and C. Brauchle.** 2001. Real-time single-molecule imaging of the infection pathway of an adeno-associated virus. Science 294:1929–1932.
51. **Snyder, R. O., C. Miao, L. Meuse, J. Tubb, B. A. Donahue, H. F. Lin, D. W. Stafford, S. Patel, A. R. Thompson, T. Nichols, M. S. Read, D. A. Bellinger, K. M. Brinkhous, and M. A. Kay.** 1999. Correction of hemophilia B in canine and murine models using recombinant adeno-associated viral vectors. Nat. Med. 5:64–70.
52. **Snyder, R. O., C. H. Miao, G. A. Patijn, S. K. Spratt, O. Danos, D. Nagy, A. M. Gown, B. Winther, L. Meuse, L. K. Cohen, A. R. Thompson, and M. A. Kay.** 1997. Persistent and therapeutic concentrations of human factor IX in mice after hepatic gene transfer of recombinant AAV vectors. Nat. Genet. 16:270–276.
53. **Tenenbaum, L., A. Chtarto, E. Lehtonen, T. Velu, J. Brotchi, and M. Levivier.** 2004. Recombinant AAV-mediated gene delivery to the central nervous system. J. Gene Med. 6(Suppl. 1):S212–S222.
54. **Thomas, C. E., T. A. Storm, Z. Huang, and M. A. Kay.** 2004. Rapid uncoating of vector genomes is the key to efficient liver transduction with pseudotyped adeno-associated virus vectors. J. Virol. 78:3110–3122.
55. **Wang, A. Y., P. D. Peng, A. Ehrhardt, T. A. Storm, and M. A. Kay.** 2004. Comparison of adenoviral and adeno-associated viral vectors for pancreatic gene delivery in vivo. Hum. Gene Ther. 15:405–413.
56. **Wang, C., C. M. Wang, K. R. Clark, and T. J. Sferra.** 2003. Recombinant AAV serotype 1 transduction efficiency and tropism in the murine brain. Gene Ther. 10:1528–1534.
57. **Wang, Z., H. I. Ma, J. Li, L. Sun, J. Zhang, and X. Xiao.** 2003. Rapid and highly efficient transduction by double-stranded adeno-associated virus vectors in vitro and in vivo. Gene Ther. 10:2105–2111.
58. **White, S. J., S. A. Nicklin, H. Buning, M. J. Brosnan, K. Leike, E. D. Papadakis, M. Hallek, and A. H. Baker.** 2004. Targeted gene delivery to vascular tissue in vivo by tropism-modified adeno-associated virus vectors. Circulation 109:513–519.
59. **Xiao, W., S. C. Berta, M. M. Lu, A. D. Moscioni, J. Tazelaar, and J. M. Wilson.** 1998. Adeno-associated virus as a vector for liver-directed gene therapy. J. Virol. 72:10222–10226.
60. **Xiao, W., N. Chirmule, S. C. Berta, B. McCullough, G. Gao, and J. M. Wilson.** 1999. Gene therapy vectors based on adeno-associated virus type 1. J. Virol. 73:3994–4003.
61. **Zhong, L., W. Li, Z. Yang, L. Chen, Y. Li, K. Qing, K. A. Weigel-Kelley, M. C. Yoder, W. Shou, and A. Srivastava.** 2004. Improved transduction of primary murine hepatocytes by recombinant adeno-associated virus 2 vectors in vivo. Gene Ther. 11:1165–1169.

Research article

Open Access

Effect of phospholipase A_2 inhibitory peptide on inflammatory arthritis in a TNF transgenic mouse model: a time-course ultrastructural study

Maung-Maung Thwin[1], Eleni Douni[2], Vassilis Aidinis[2], George Kollias[2], Kyoko Kodama[3], Kazuki Sato[3], Ramapatna L Satish[4], Ratha Mahendran[4] and Ponnampalam Gopalakrishnakone[1]

[1]Venom & Toxin Research Program, Department of Anatomy, National University of Singapore, Singapore
[2]Institute of Immunology, Biomedical Sciences Research Center, Al Fleming, 34 Al Fleming Street, 16672 Vari, Greece
[3]Fukuoka Women's University, Fukuoka 813-8529, Japan
[4]Department of Surgery, Faculty of Medicine, National University of Singapore, Singapore

Corresponding author: Ponnampalam Gopalakrishnakone, antgopal@nus.edu.sg

Received: 19 Jan 2004 Revisions requested: 6 Feb 2004 Revisions received: 12 Mar 2004 Accepted: 25 Mar 2004 Published: 28 Apr 2004

Arthritis Res Ther 2004, **6**:R282-R294 (DOI 10.1186/ar1179)

Abstract

We evaluated the therapeutic effect of secretory phospholipase A_2 ($sPLA_2$)-inhibitory peptide at a cellular level on joint erosion, cartilage destruction, and synovitis in the human tumor necrosis factor (TNF) transgenic mouse model of arthritis. Tg197 mice ($N = 18$) or wild-type ($N = 10$) mice at 4 weeks of age were given intraperitoneal doses (7.5 mg/kg) of a selective $sPLA_2$ inhibitory peptide, P-NT.II, or a scrambled P-NT.II (negative control), three times a week for 4 weeks. Untreated Tg197 mice ($N = 10$) were included as controls. Pathogenesis was monitored weekly for 4 weeks by use of an arthritis score and histologic examinations. Histopathologic analysis revealed a significant reduction after P-NT.II treatment in synovitis, bone erosion, and cartilage destruction in particular. Conspicuous ultrastructural alterations seen in articular chondrocytes (vacuolated cytoplasm and loss of nuclei) and synoviocytes (disintegrating nuclei and vacuoles, synovial adhesions) of untreated or scrambled-P-NT.II-treated Tg197 mice were absent in the P-NT.II-treated Tg197 group. Histologic scoring and ultrastructural evidence suggest that the chondrocyte appears to be the target cell mainly protected by the peptide during arthritis progression in the TNF transgenic mouse model. This is the first time ultrastructural evaluation of this model has been presented. High levels of circulating $sPLA_2$ detected in untreated Tg197 mice at age 8 weeks of age were reduced to basal levels by the peptide treatment. Attenuation of lipopolysaccharide- and TNF-induced release of prostaglandin E_2 from cultured macrophage cells by P-NT.II suggests that the peptide may influence the prostaglandin-mediated inflammatory response in rheumatoid arthritis by limiting the bioavailability of arachidonic acid through $sPLA_2$ inhibition.

Keywords: peptide, secretory phospholipase A_2 inhibition, rheumatoid arthritis, TNF transgenic mouse model, ultrastructural alterations

Introduction

Secretory phospholipase A_2 ($sPLA_2$) is a key enzyme in the production of diverse mediators of inflammatory and related conditions [1]. Because of the crucial role it plays in inflammatory diseases such as rheumatoid arthritis (RA) [2], $sPLA_2$ is referred to as inflammatory PLA_2 [3]. High levels of $sPLA_2$ have been found in synovial tissues and fluid from patients with RA [2,4]. Purified synovial PLA_2 can elicit an inflammatory arthritogenic response when injected into the joint space of healthy rabbits and rats [5,6]. It has been reported that $sPLA_2$ expression parallels the severity of the inflammatory process with lack of enhancement of cytosolic phospholipase A_2 ($cPLA_2$) mRNA in an adjuvant arthritis model, thus indicating the pathogenic role played by $sPLA_2$ [7]. Colocalization studies using primary synovial fibroblasts from RA patients have also suggested $sPLA_2$ as a critical modulator of cytokine-mediated synovial inflammation in RA [8]. As a result of its important role in the inflammatory response, inhibition of $sPLA_2$ is a target for the treatment of inflammatory diseases. Inhibition of $sPLA_2$

AA = arachidonic acid; ANOVA = analysis of variance; AS = arthritis score; $cPLA_2$ = cytosolic phospholipase A_2; DMSO = dimethyl sulfoxide; HS = histopathologic score; LPS = lipopolysaccharide; PGE = prostaglandin E; PIP = phospholipase inhibitor from python; RA = rheumatoid arthritis; r-ER = rough endoplasmic reticulum; SEM = standard error of the mean; $sPLA_2$ = secretory phospholipase A_2; Tg = transgenic; TNF = tumor necrosis factor.

could result in suppression of several classes of proinflammatory lipids such as prostaglandins, leukotrienes, platelet-activating factor, and lysophospholipid [1].

Elevated levels of circulating $sPLA_2$ are usually associated with high blood levels of proinflammatory cytokines [9], which are used as an indicator of the extent of systemic inflammation [10,11]. $sPLA_2$ has been shown to activate the production of proinflammatory cytokines in blood and synovial fluid monocytes [12], suggesting that the two can cooperate to promote inflammation by enhancing each other's secretion. $sPLA_2$ may act on the cells stimulated with such cytokines, leading to augmentation of the inflammatory responses. The fact that cotransgenic $sPLA_2$ and tumor necrosis factor α (TNF-α) mice show more extensive swelling than TNF-α transgenic mice [13] may be evidence in support of a possible synergism between $sPLA_2$ and TNF. Hence, inhibition of $sPLA_2$ may further help to suppress inflammation in RA by blocking the formation of proinflammatory cytokines.

A significant reduction of the inflammatory response has been reported in animals injected with natural or synthetic $sPLA_2$ inhibitors [14,15]. Two families of endogenous proteins, namely lipocortins and uteroglobin, have been shown to possess anti-inflammatory properties due to their ability to inhibit $sPLA_2$. Synthetic peptides called antiflammins derived from these proteins are one of the most potent classes of anti-inflammatory agents identified to date [16]. A recombinant protein termed PIP (phospholipase inhibitor from python), which we have expressed from the liver of a nonvenomous snake, *Python reticulatus* [17], exhibits *in vivo* anti-inflammatory activity that correlates well with its *in vitro* inhibitory potency towards $sPLA_2$. In a clinically relevant model of postsurgical peritoneal adhesion, the peptide analog P-PB.III, which has a fragment of an anti-inflammatory protein PIP included in its sequence, exhibits stronger *in vivo* anti-inflammatory activity than that displayed by antiflammin [18]. Further screening of the PIP amino acid sequence provides us with a new peptide with improved potency. This new 17-mer peptide ^{56}LGRVDIHVWDGVYIRGR^{72} is a selective inhibitor of human $sPLA_2$-IIA, with an amino acid sequence corresponding to residues 56–72 of the native protein PIP. It significantly reduces high levels of $sPLA_2$ detected in rat hippocampal homogenates after intracerebroventricular injections of a neurotoxin, kainic acid [19]. These findings establish that peptides or recombinant proteins that inhibit $sPLA_2$, or their peptide derivatives, are highly attractive candidates for clinical development as anti-inflammatory agents.

The present study was designed to investigate the effect of a selective $sPLA_2$-inhibitory peptide, P-NT.II, on ultrastructural changes of ankle-joint synovitis, cartilage degradation, and bone erosion in the Tg197 TNF transgenic mouse model of arthritis [20], and to assess the effects of peptide intervention on the clinical and histologic indices of RA.

Materials and methods

Animals

The generation and characterization of Tg197 human TNF transgenic mice have been previously described [20]. Tg197 mice generated on CBA × C57BL/6 genetic backgrounds and littermate controls were bred and maintained at the animal facilities of the Biomedical Sciences Research Center, Alexander Fleming, Athens, Greece, under specific-pathogen-free conditions. All of the Tg197 mice typically developed polyarthritis 3–4 weeks after birth, whereas nontransgenic (wild-type) mice remained normal. Mice were given conventional oral food and water *ad libitum*. All procedures involving animals were in compliance with the Declaration of Helsinki principles.

Experimental protocol

A total of 44 weight-matched mice (34 Tg197 and 10 nontransgenic wild-type littermates) were divided into six groups for subsequent gross observations and histopathologic analyses – untreated Tg197 group ($N = 10$), P-NT.II-treated Tg197 group ($N = 18$), scrambled-P-NT.II-treated Tg197 group ($N = 6$), P-NT.II-treated wild-type group ($N = 4$), scrambled-P-NT.II-treated wild-type group ($N = 4$), and Tg197 baseline group – just before the treatment at 4 weeks of age ($N = 4$). Nontransgenic mice were given the same dose of P-NT.II or scrambled P-NT.II, and the same regimen of treatment, as the Tg197 mice.

Peptide synthesis and administration

P-NT.II (test peptide) and the scrambled P-NT.II (negative control peptide) were synthesized using the solid-phase method with 9-fluorenylmethoxy carbonyl chemistry and were purified and validated as described elsewhere [18]. They were stored lyophilized at -20°C in sealed tubes and were dissolved freshly before use in 0.1% dimethyl sulfoxide (DMSO). Each Tg197 or wild-type mouse was given intraperitoneal injections of P-NT.II or the scrambled P-NT.II (7.5 mg/kg) in 50 μl of vehicle (0.1% final DMSO concentration), three times a week for 4 weeks (i.e. from age 4–8 weeks).

Clinical assessment

This was done by gross observations based on bodyweight measurements and arthritis scoring, which were done twice weekly from 4 weeks (baseline) to 8 weeks of age (end of the study), after which all the animals were killed by CO_2 inhalation. The level of severity of clinical arthritis was evaluated based on an arthritis score (AS) taken on both ankle joints. Average scores on a scale of 0–3 were used; 1 = mild arthritis (joint swelling); 2 = moderate arthritis (severe joint swelling and deformation, no grip

strength); 3 = severe arthritis (ankylosis detected on flexion, and severely impaired movement) [21].

Histologic examinations

The whole ankle joints harvested from the right side of each mouse were fixed overnight in 10% formalin, decalcified in 30% citrate-buffered formic acid for 3 days at 4°C, dehydrated in a graded series of methanol and xylene, and then embedded in paraffin. Thin sections (6 μm thick) were stained with hematoxylin and eosin, and histopathologic scorings performed under the light microscope (Leitz Aristoplan) by a blinded observer. The histopathologic score (HS) was evaluated [21] using a scale of severity ranging from 1 to 4, where 1 = hyperplasia of the synovial membrane and presence of polymorphonuclear infiltrates, 2 = pannus and fibrous tissue formation and focal subchondral bone erosion, 3 = articular cartilage destruction and bone erosion, and 4 = extensive articular cartilage destruction and bone erosion.

Scoring of joint parameters

Arbitrary scores were used to assess the extent of synovitis, cartilage destruction, and bone erosion. Semiquantitative scores from 0 to 4 were used for each histopathologic parameter [22]. Synovitis: 0 = normal; 1 = mild synovial hypertrophy (<5 cell layers) with few inflammatory cells; 2 = moderate synovial hypertrophy (<20 cell layers) with accumulation of inflammatory cells into intrasynovial cysts; 3 = pannus and fibrous tissue formation; and 4 = pannus and fibrous tissue formation on both sides of the ankle joint. Cartilage damage: 0 = intact; 1 = minor (<10%); 2 = moderate (10–50%); 3 = high (50–80%); and 4 = severe (80–100%). Bone erosions: 0 = normal; 1 = mild (focal subchondral erosion); 2 = moderate (multiple subchondral erosions); 3 = high (as above + focal erosion of talus); and 4 = maximum (multiple erosions of tarsal and metatarsal bones).

Transmission electron microscopy

Ankle joints dissected from the left hind leg of each mouse were split open longitudinally through the midline between the tibia and the talus, prefixed overnight with 2.5% glutaraldehyde in phosphate buffer, pH 7.4, and rinsed with the buffer. After they had been postfixed with 1% osmium tetroxide in phosphate buffer for 2 hours, they were dehydrated in a graded series of ethanol and embedded in epoxy resin (Araldite). Semithin sections (1.0 μm) were cut and stained with methylene blue to reveal their orientation for ultrathin sectioning and for histopathologic scoring under the light microscope. Ultrathin sections (80–90 nm) were then cut with an ultramicrotome (Ultracut E; Riechert-Jung, Leica, Vienna, Austria), mounted on copper grids, counterstained with uranyl acetate and lead citrate, and evaluated in the electron microscope (CM120 Biotwin; FEI Company, Electron Optics, Eindhoven, The Netherlands).

Measurement of serum PLA2

$sPLA_2$ was measured in the serum of transgenic (Tg197) mice and nontransgenic wild-type controls, using an *Escherichia coli* membrane assay as described previously [18]. In brief, [^{3}H]arachidonate-labeled *E. coli* membrane suspension (5.8 μCi/μmol, PerkinElmer Life Sciences, Inc, Boston, MA, USA) was used as substrate, and 25 mM $CaCl_2$-100 mM Tris/HCl (pH 7.5) as assay buffer. The reaction mixture, containing substrate (20 μl) and either purified human synovial $sPLA_2$ standard (1–80 ng/ml; Cayman Chemical Company, Ann Arbor, MI, USA) or serum (10 μl), in a final volume of 250 μl in assay buffer, was incubated at 37°C for 1 hour, and the reaction was terminated with 750 μl of chilled phosphate-buffered saline containing 1% bovine serum albumin. Aliquots (500 μl) of the supernatant were then taken, for measurement of the amount of [^{3}H]arachidonate released from the *E. coli* membrane using liquid scintillation counting (LS 6500 Scintillation Counter; Beckman Inc., Fullerton, CA, USA). The amount of $sPLA_2$ present in the serum was calculated from the standard curve and is expressed as ng/ml ± SEM.

Cell culture

The murine macrophage cell line J774 (American Type Culture Collection, Manassas, VA, USA) was cultured at 37°C in humidified 5% CO_2/95% air in Dulbecco's modified Eagle's medium containing 10% fetal bovine serum, 2 mM glutamine, 20 mM HEPES, 100 IU/ml penicillin, and 100 μg/ml streptomycin. After growing to confluence, the cells were dislodged by scraping, plated in 12 culture wells at a density of 5×10^5 cells/ml per well, and allowed to adhere for 2 hours. Thereafter, the medium was replaced with fresh medium containing lipopolysaccharide (LPS) (2 μg/ml) and one of the PLA_2 inhibitors (P-NT.II, scrambled P-NT.II, or LY315920 [Lilly Research Laboratories, Indianapolis, IN, USA], dissolved in DMSO [final concentration 0.1% v/v]). Peptides were tested at various concentrations ranging from 0.01 to 40 μM. After incubation in 5% CO_2/95% air at 37°C for 20 hours, culture medium supernatants were collected and stored frozen (-80°C) until use. In parallel experiments, cells were stimulated with mouse recombinant TNF (10 ng/ml; Sigma, St. Louis, MO, USA) for 20 hours, in the presence or absence of 10 μM P-NT.II or LY315920 dissolved in DMSO (0.1% final concentration). Culture medium supernatants were collected after centrifugation (10,000 ***g***, 4°C, 15 min) and stored at -80°C prior to measurement of prostaglandin E_2 (PGE_2).

Cell viability assays

XTT (sodium 3'-[(phenyl amine carboxyl)-3,4-tetrazolium]-bis(4-methoxy-nitro) benzene sulfonic acid hydrate) Cell Proliferation Kit II (Roche Applied Science) was used to assess the possible cytoxic effect of the peptide P-NT.II on the mouse macrophage J774 cell line.

Measurement of PGE_2

PGE_2 (EIA kit-monoclonal; Cayman) concentrations were measured in the cell-culture supernatants in accordance with the manufacturer's instructions.

Statistical analysis

Statistical analyses were performed using GraphPad Prism software to calculate the means and SEMs. Group means were compared by using one-way analysis of variance (ANOVA), followed by Bonferroni's multiple comparison post test to identify statistically significant differences (i.e. $P < 0.05$).

Results

Gross histologic findings

Figure 1 shows the histologic features of ankle joints of Tg197 mice in the untreated, P-NT.II-treated, and scrambled-P-NT.II-treated groups. Gross histologic findings of the three experimental groups are summarized in Table 1. At 8 weeks of age, ankle joints from the untreated Tg197 group were moderately (90% with HS 3) to severely (10% with HS 4) damaged, with pannus and fibrous tissue formation and focal subchondral bone erosion. Articular cartilage destruction and bone erosion were observed in 90% of those joints (Fig. 1a,1b). In contrast, all the articular cartilage surfaces and associated synovial linings of the ankle joints of the P-NT.II-treated group at 2 weeks post-treatment (i.e. age 6 weeks) were only mildly affected (HS 2), with no evidence of cartilage or bone erosion (Fig. 1c), and 25% of joints were affected moderately (HS 3) at 4 weeks post-treatment (i.e. age 8 weeks) (Fig. 1d). In contrast, 83.3% of joints of scrambled-P-NT.II-treated Tg197 mice at 8 weeks of age were moderately damaged (HS 3) (Fig. 1e,1f), with histologic features similar to those of the untreated Tg197 mice. Although the disease, as assessed by the HS, was significantly lower in the P-NT.II-treated group than in the untreated or scrambled-P-NT.II-treated groups, visual disease scores (ASs) did not correlate well with the HS. In contrast to HSs, ASs of mice treated with P-NT.II did not significantly differ from those of the untreated or scrambled-P-NT.II-treated group (Fig. 2).

Analytical HS

To assess specific effects of the peptide P-NT.II on synovitis, cartilage destruction, and bone erosion, we conducted a semiquantitative scoring analysis for each of these pathologic parameters. P-NT.II treatment in Tg197 mice resulted in a significant reduction ($P < 0.05$) in all three analytical HSs as compared with those of untreated or scrambled-P-NT.II-treated Tg197 mice, which all developed synovitis with severe articular cartilage degradation and bone erosions (Fig. 3). Statistical analysis revealed a greater beneficial effect of P-NT.II on cartilage destruction and bone erosion ($^{**}P < 0.01$ versus untreated or scrambled-P-NT.II-treated groups for both parameters) than on synovitis ($^{*}P < 0.05$ versus untreated or scrambled-P-NT.II-treated groups).

Ultrastructural changes in articular cartilage

Articular cartilage in the ankle joints of all untreated Tg197 mice was generally damaged at 8 weeks of age (Fig. 4c,4d,4e,4f) as compared with normal morphology seen in control, wild-type mice (Fig. 4a). No significant ultrastructural changes in the nucleus and plasma membrane were noted at the cellular level in the articular cartilage of untreated Tg197 mice at age 4 weeks (baseline) except for some minor changes including vacuoles, dilated cisternae, and the presence of granular materials seen inside the cytoplasm (Fig. 4b). In the 8-week-old mice, the chondrocytes on the surface of the superficial cartilage layer had become necrotic, with alterations of cartilage developed in most cases (Fig. 4c,4d,4e,4f). The cell body and nucleus of some chondrocytes became large and rounded, resulting in vacuolation, and the cytoplasm was transparent, with an accumulation of intracytoplasmic filaments (Fig. 4c). Degenerating chondrocytes with greatly vacuolated cytoplasm and pyknotic nuclei (Fig. 4d), and chondrocytes with complete loss of nuclei and disrupted rough endoplasmic reticulum (r-ER) (Fig. 4e,4f), were also observed. In contrast, the ultrastructural features of chondrocytes 1–4 weeks after P-NT.II treatment (i.e. age 5–8 weeks; Fig. 5a) did not substantially differ from those seen in the joints of normal wild-type mice (Fig. 4a). Most of them had a prominent nucleus, lined by plasma membrane with short cytoplasmic protrusions, and vacuoles, r-ER, and mitochondria in the cytoplasm. The ultrastructure of chondrocytes of the scrambled-P-NT.II-treated joints at 8 weeks of age (Fig. 5b) were more or less similar to those described for untreated Tg197 mice with degenerating features such as the greatly vacuolated cytoplasm and pyknotic nuclei (cf. Fig. 4d) or loss of nucleus, disrupted r-ER (cf. Fig. 4f), and swollen mitochondria with distorted cristae (cf. Fig. 4c).

Ultrastructural changes in synovium

The early response of the synovial membrane in the untreated Tg197 mice at age 4 weeks (baseline) was synovial hyperplasia, with the presence of type A and B synovial cells along with inflammatory cells such as lymphocytes, macrophages, and mast cells. Type A cells were similar to macrophage cells and were characterized by many vesicles, vacuoles, and a higher number of cell processes. Type B cells were similar to fibroblast cells and contained small vesicles and r-ER. The later response (at ≥ 5 weeks of age) included degeneration of synovial cells, with swollen mitochondria and cell fragmentations. In areas of high inflammation, the synovial tissue (mostly type A cells) had proliferated into the articular cavity (Fig. 6a). Type A and B cells in the synovium were no longer distinguishable at age 6 weeks and thereafter. The synovial membrane was lined by closely packed elongated synoviocytes which

Figure 1

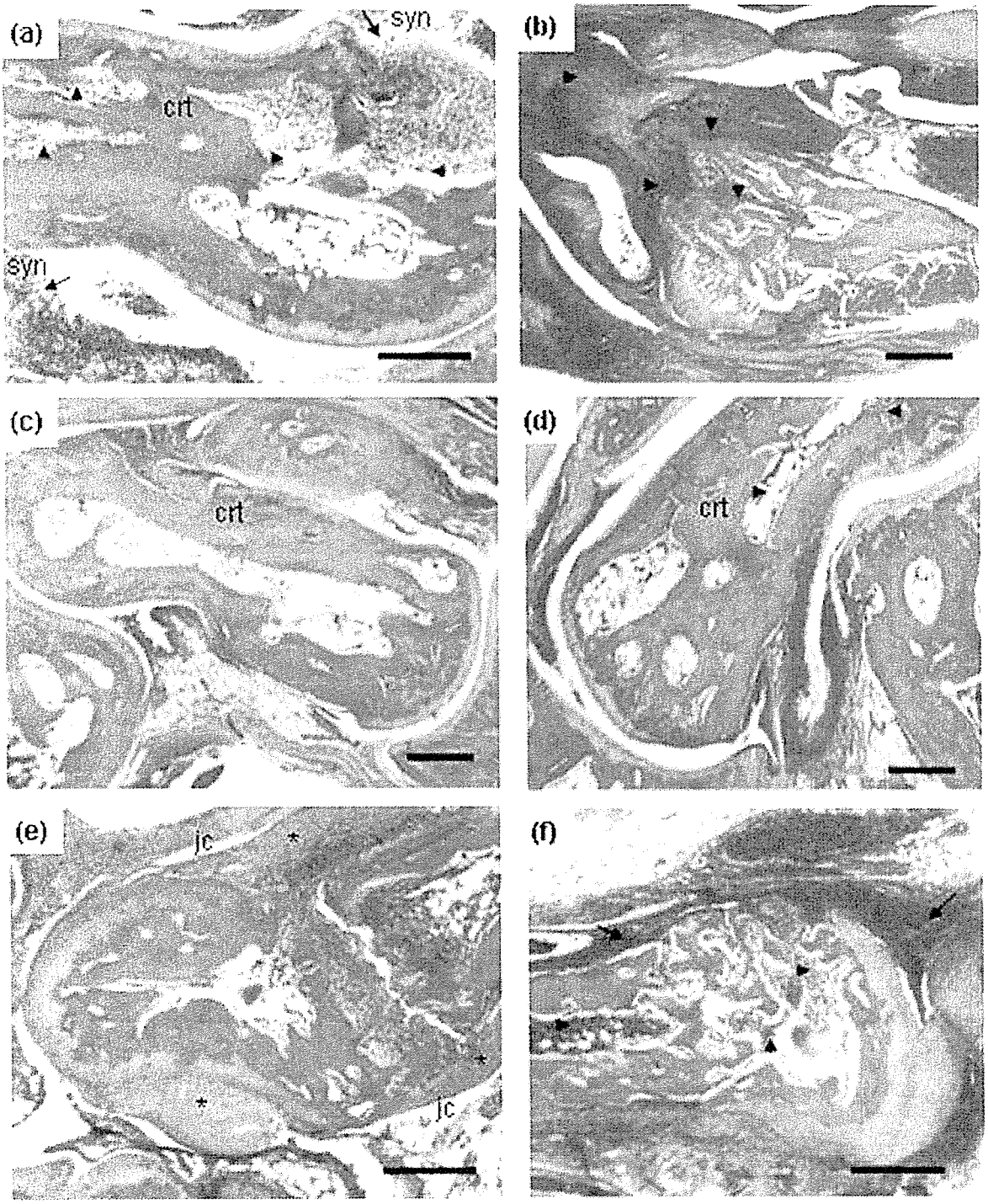

Histologic findings in the ankle joints of Tg197 mice. **(a,b)** Untreated mice: (a) partially altered articular cartilage (crt) with bone erosion (arrowhead), and presence of inflammatory infiltrates (arrow) in the synovial (syn) tissue; (b) extensive articular cartilage destruction and bone erosion (arrowhead). **(c,d)** P-NT.II-treated mice: (c) minor cartilage changes (crt) with absence of bone erosion; (d) focal articular cartilage destruction (crt) and minor bone erosion (arrowhead). **(e,f)** Mice treated with scrambled P-NT.II: (e) the joint cavity (jc) is lined with synovitis (*); (f) cartilage destruction and bone erosion (arrowhead) are present, along with inflammatory infiltrates (arrow). Nontransgenic controls showed normal joint structures throughout the study (data not shown). (Hematoxylin & eosin staining; original magnification ×25 in a, e, f; ×10 in b, c, d. Bars = 500 μm).

Table 1

Histopathologic assessment of ankle joints

Treatment	Time course (weeks)	Joints scored	% of total at indicated HS			HS (Mean ± SEM)
			HS 2	HS 3	HS 4	
None	4	10	0	90.0	10	3.30 ± 0.11[a]
P-NT.II*	1	4	100	0	0	2.12 ± 0.12
P-NT.II*	2	4	100	0	0	2.37 ± 0.12
P-NT.II*	3	4	75	25	0	2.50 ± 0.20
P-NT.II*	4	4	75	25	0	2.62 ± 0.31[b]
Scrambled-P-NT.II-treated (negative control peptide)	4	6	16.7	83.3	0	3.25 ± 0.17[c]

*Tg197 mice injected (intraperitoneally) with the test peptide P-NT.II were killed at weekly intervals ($N = 4$ per group) for 4 weeks and their ankle joints examined. For untreated and negative control groups, ankle joints were harvested only at the end of the 4 weeks' study course for one-time examination. Histologic scoring was performed semiquantitatively by a blinded examiner. HS 2 = pannus and fibrous tissue formation and focal erosion of subchondral bone; HS 3 = articular cartilage destruction and bone erosion; HS 4 = extensive articular cartilage destruction and bone erosion. *a* versus *b*, *b* versus *c* = significantly different ($P < 0.05$; one-way analysis of variance with Bonferroni's multiple comparison test). HS, histopathologic score; SEM, standard error of the mean.

were sealed by junctional systems of the adherent type (Fig. 6b). Large amounts of fibrin deposition on the synovial surface could be seen, and the two opposing, flattened synoviocytes with fibrin between them indicated the existence of synovial adhesion (Fig. 6d). Also, degenerating synoviocytes with disintegrating nuclei and vacuolated cytoplasm were randomly seen in the synovium (Fig. 6c). Synoviocytes appeared flattened, and partially degranulated mast cells were seen under the synovium (Fig. 6e).

P-NT.II treatment tended to decrease the number of inflammatory cells, with less degeneration of synovial cells and cell fragmentation seen in the joints of the treated group (Fig. 7b). The peptide P-NT.II retained at least the basic structural organization of the synovial membrane seen in the control wild-type mice (Fig. 7a), while the synoviocytes from mice treated with scrambled P-NT.II (Fig. 7c) were structurally indistinguishable from those seen in untreated joints (cf. Fig. 6). In those joints, the synovial cells were seen lining up close together, and many cell fragments resulting from degenerating cells were present in the synovium, along with infiltrating mast cells (Fig. 7c).

Serum levels of $sPLA_2$

In a time-course study to evaluate the specific effect of peptide in modulating the serum $sPLA_2$ levels in Tg197 mice (Fig. 8), P-NT.II significantly suppressed the circulating $sPLA_2$ in the mice at age 8 weeks ($P < 0.05$), by comparison with the serum levels of the untreated mice of same age. In contrast, the circulating $sPLA_2$ of scrambled-P-NT.II-treated and untreated Tg197 mice at age 8 weeks were not significantly different ($P > 0.05$), thus indicating the specific effect of the peptide P-NT.II on $sPLA_2$ levels.

PGE_2 release from cultured macrophages

The suppressive effect of P-NT.II and $sPLA_2$-selective inhibitor LY315920 (Lilly) on LPS- and TNF-stimulated PGE_2 production was examined in mouse macrophage cell cultures (Fig. 9). Production of PGE_2 in the medium increased approximately sixfold from the basal level of 55 ± 6 pg/ml to 320 ± 35 and 330 ± 11 pg/ml (mean ± SD, $N = 5$), after 20 hours' stimulation of cultured cells with LPS (2 μg/ml) (Fig. 9a) or TNF (10 ng/ml) (Fig. 9b), respectively. When the inhibitors were coincubated with either LPS- or TNF-stimulated macrophages in the medium, both P-NT.II and LY315920 (final concentration 10 μM) dose-dependently inhibited PGE_2 production, with estimated IC_{50} values of 25 and 30 μM, respectively. In contrast, scrambled P-NT.II (negative control) showed no inhibitory effect on either LPS- or TNF-induced PGE_2 release in the culture medium. Neither the peptide nor LY315920 affected the cellular viability, when tested by XTT assay kit at the highest concentration (40 μM) used in culture experiments ($E_{492\,nm}$ values of 0.89 ± 0.02, 0.84 ± 0. 021, and 0.92 ± 0.019 for untreated, P-NT.II-treated, and LY315920-treated cells, respectively).

Discussion

Here we report the beneficial effect of peptide treatment, and the ultrastructural changes seen at the cellular level in the articular cartilage and synovium of the ankle joints of TNF transgenic Tg197 mice treated with the anti-inflammatory peptide P-NT.II. While several studies have previously been carried out on the early ultrastructural changes in other animal models of experimental arthritis [23-25], no morphological evaluations in this TNF transgenic mouse model of RA have yet been available, in either the absence or the presence of therapeutic intervention.

Figure 2

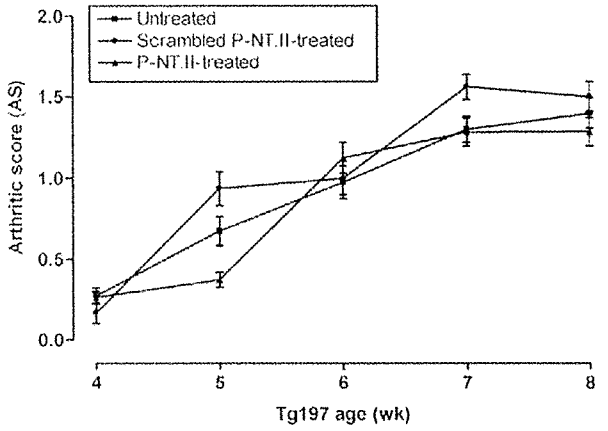

The arthritis score (AS) in Tg197 mice changes with time course. The AS was determined on both ankle joints of each mouse by a blinded examiner, using a scale of 0–3 as described in Materials and methods. Values are the mean ± SEM.

Figure 3

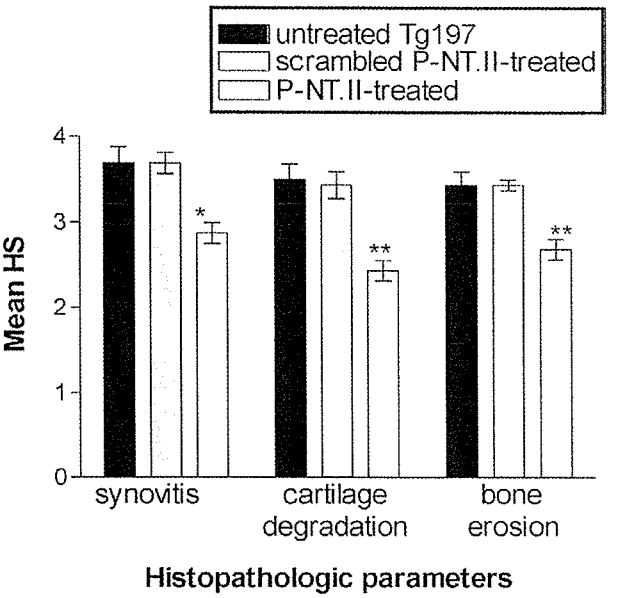

Histopathologic score (HS) analysis of various histopathologic parameters in Tg197 mice. Synovitis, cartilage degradation, and bone erosion were semiquantitatively assessed in the ankle joints of Tg197 mice that were untreated, treated with P-NT.II, or treated with scrambled-P-NT.II ($N = 4$/group) at 4 weeks post-treatment (i.e. age 8 weeks). The HS indicates a protective effect of P-NT.II in all three histopathologic parameters of arthritis. Statistical analysis revealed a greater beneficial effect of P-NT.II on cartilage destruction and bone erosion (**$P < 0.01$ versus untreated or scrambled-P-NT.II-treated groups for both parameters) than on synovitis (*$P < 0.05$ versus untreated or scrambled-P-NT.II-treated groups).

The lesions in the TNF transgenic mouse model of arthritis we used in the present study histologically and ultrastructurally resemble RA lesions [26], with synovial proliferation along the articular surface and subsequent invasion with erosion of the articular cartilage and subchondral bone. Although visual disease scores (ASs) did not show any significant difference between P-NT.II-treated and control (scrambled-P-NT.II-treated or untreated) groups, the results obtained from gross histologic analysis (Table 1) and semiquantitative analysis of pathologic parameters (Fig. 3) clearly demonstrate the beneficial effect of peptide treatment in preventing synovitis, cartilage destruction, and bone erosion. Similar discrepancies between AS and HS have also been reported in TNF-transgenic and other experimental models of arthritis. Redlich and colleagues [27] recently reported a protective effect of osteoprotegerin treatment on bone damage in Tg197 mice, with lack of any beneficial effect on the clinical symptoms. In another experimental model of passive collagen-induced arthritis using JNK2-deficient mice, it has been shown that clinical symptoms appear to be slightly more severe than HS despite significant reductions in joint destruction due to preservation of the articular cartilage [28]. It seems, therefore, that preservation of the bone structure may not always correlate with the clinical symptoms. The striking difference observed in the ultrastructural features of the articular cartilage and synovial membrane in our animal model before and after peptide treatment did confirm that P-NT.II administered as an exogenous drug in this TNF transgenic mouse model of RA was able to improve the overall morphology and the cellular component of the synovium, and of the cartilage in particular.

Ultrastructural changes of ankle articular cartilage and synovium in Tg197 mice were evaluated using transmission electron microscopy, before and during the 4-week course of treatment. Histologically, we observed an apparent suppression of pannus formation and minimal erosive damage to the articular cartilage and subchondral bone. At 1–4 weeks post-treatment with peptide (i.e. at age 5–8 weeks), the number of inflammatory cells in the synovial tissue was reduced as early as 1 week after initiation of treatment, and the structural organization of the synovial membrane of the ankle joint appeared less modified. In the P-NT.II-treated group, lesions such as synovial adhesions, cell fragmentation due to degeneration of synoviocytes, and dilation of the r-ER and distorted cristae of type B cells were less obvious than in the untreated or scrambled-P-NT.II-treated groups. In our cell-culture experiments using mouse macrophages, P-NT.II has been found to dose-dependently inhibit LPS- or TNF-induced PGE_2 production, with a potency equal to that of a potent and selective $sPLA_2$ inhibitor, LY315920 [29]. It is possible that P-NT.II may modulate ultrastructural modifications to the synovium by reducing the bioavailability of arachidonic acid (AA) through $sPLA_2$ inhibition, and

Figure 4

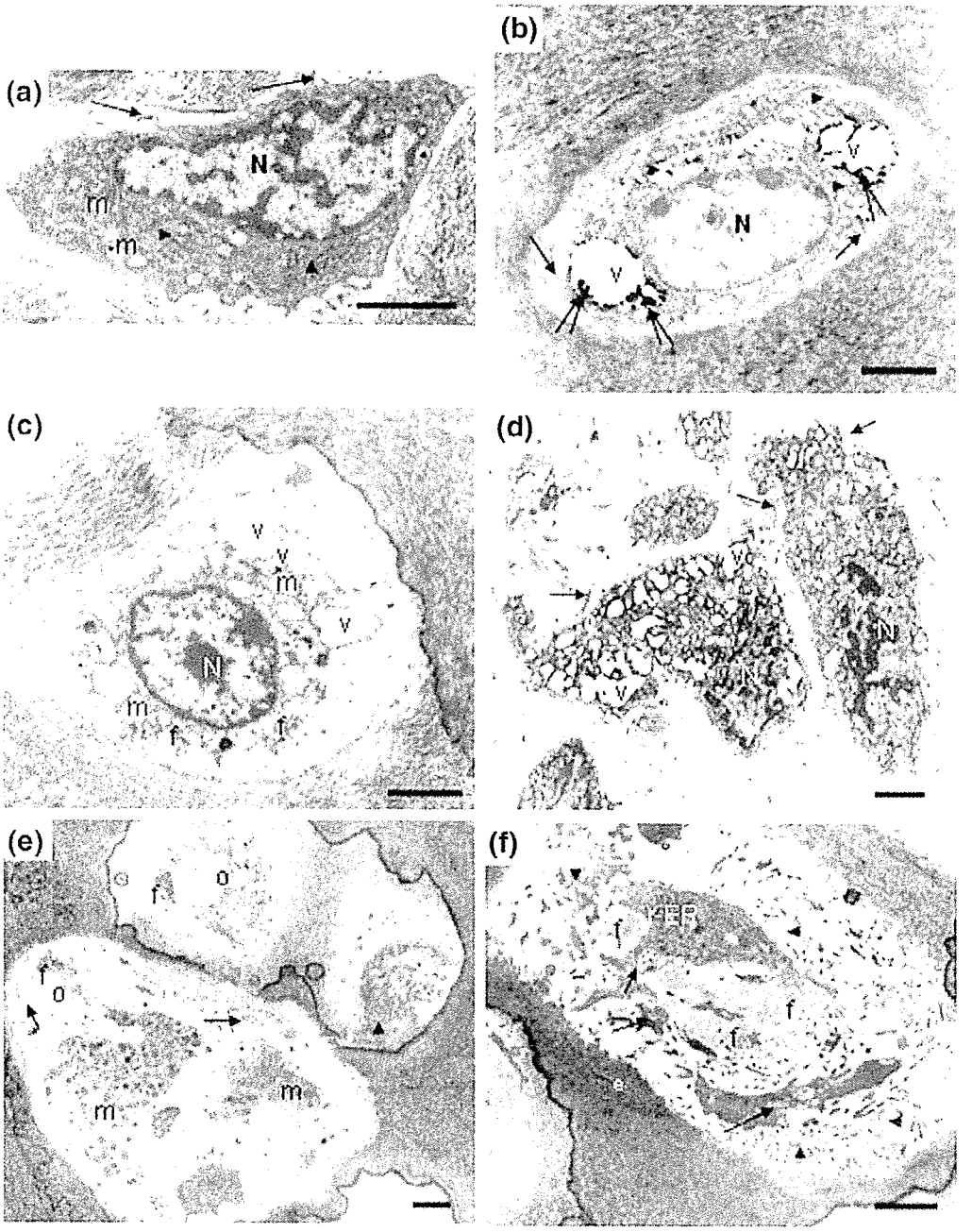

Chondrocytes of wild-type controls and untreated Tg197 mice. **(a)** Wild-type control at age 8 weeks: nucleus (N), plasma membrane with short cytoplasmic protrusions (arrow), rough endoplasmic reticulum (r-ER) (arrowhead), and mitochondria (m); **(b)** untreated Tg197 mouse at age 4 weeks: nucleus (N) and plasma membrane with cytoplasmic thin protrusions (arrow) appear normal, while the cytoplasm shows vacuoles (v) with granular materials inside (double arrow) and dilated cisternae (arrowhead). **(c-f)** Untreated Tg197 mouse at age 8 weeks: degenerating chondrocytes showing the following: (c) transparent cytoplasm with nucleus (N) and an accumulation of intracytoplasmic filaments (f), vacuoles (v) and mitochondria (m) with distorted cristae; (d) greatly vacuolated cytoplasm (v), and pyknotic nuclei (N) with cytoplasmic projections coming apart from the cell (arrow); (e) cell organelles from disintegrated cells (o), mitochondria (m), bundles of densely packed collagen fibres (arrowhead), small residues of intermediate filaments (f), and broken cellular processes (arrow); (f) swollen and disrupted r-ER, and bundles of thickened intermediate filaments (f). Basement membrane, cytoplasmic organelles (arrow), and cellular processes (arrowhead) were also fragmented. Electron-dense areas (e) are seen in the intercellular matrix. $N = 4$ joints; mean percentage of degenerating chondrocytes = 40% and 80% of total at 4 and 8 weeks of age, respectively. Bars = 2 μm.

Figure 5

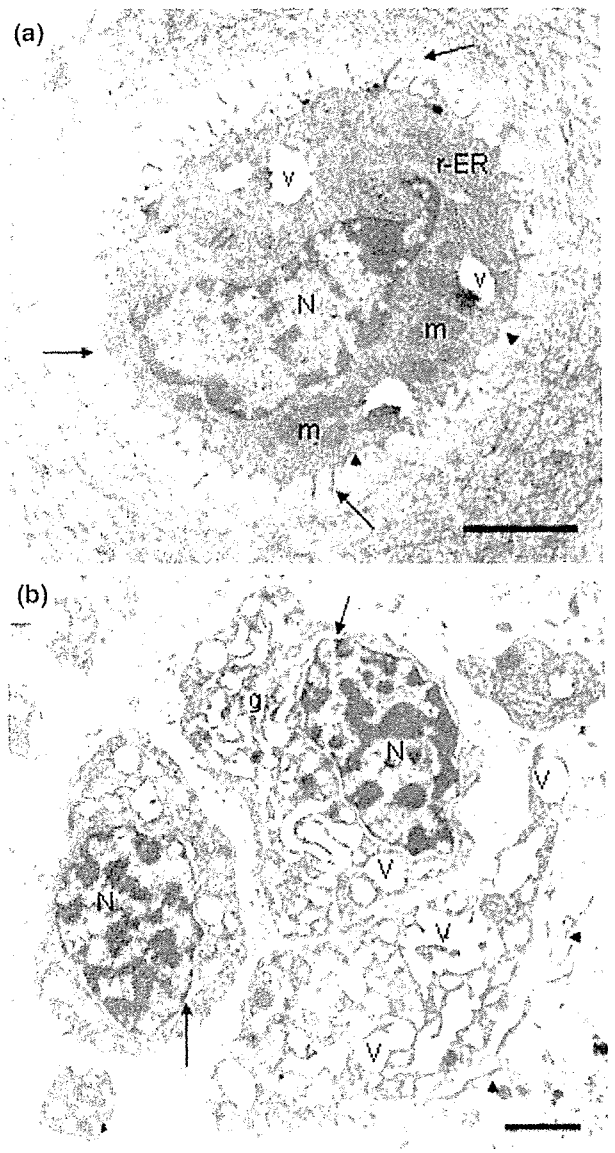

Chondrocytes of treated Tg197 mice. **(a)** Chondrocytes of P-NT.II-treated Tg197 mice at 5–8 weeks of age (i.e. 1–4 weeks post-treatment) were similar to those described for normal chondrocytes, with almost intact nucleus (N), basement membrane (arrowhead), and cytoplasmic organelles – vacuoles (v), rough endoplasmic reticulum (r-ER), mitochondria (m); **(b)** Most chondrocytes of Tg197 mice treated with scrambled P-NT.II at age 8 weeks (i.e. 4 weeks post-treatment) were degenerated, with vacuolated cytoplasm (v), a disrupted Golgi complex (g), pyknotic nuclei (N) with a well-defined, enlarged perinuclear space (arrows), and cytoplasmic projections broken from the cell (arrowhead). $N = 4$ joints/group; mean percentage of degenerating chondrocytes at age 8 weeks = 20% and 75% of total in (a) and (b), respectively. Bars = 2 μm.

suppress the severity of the prostaglandin-mediated inflammatory response in the synovium.

The ultrastructural features of the articular cartilage observed in this human TNF transgenic mouse model of RA suggest that the chondrocyte may be one of the important targets of the peptide intervention in modulating the progression of the joint erosion. Our extensive histopathologic analysis of joints in the Tg197 TNF model in this study (Fig. 3) has revealed both articular cartilage destruction and subchondral bone erosion at the advanced stages of disease (i.e. 8 weeks of age). Similar severe cartilage destruction in Tg197 mice at 7–8 weeks of age has previously been shown as evidenced by the loss of safranin-O staining [22]. Massive cartilage and subchondral bone erosion in the joints is the hallmark of inflammatory arthritis in the TNF transgenic mouse model [30]. At 3–4 weeks post-treatment (i.e. at 7–8 weeks of age), P-NT.II significantly reduced chondrocyte necrobiosis, which was frequently seen in the proximity of invading synovium in untreated controls at same age. It is possible that $sPLA_2$ might be involved in cartilage destruction in the TNF-transgenic model. $sPLA_2$ found in the synovial fluid has been reported to originate from chondrocytes and not from the synovial lining or inflammatory cells [31]. Human articular chondrocytes synthesize and constitutively release $sPLA_2$, and are therefore suggested to be responsible for the high concentration of $sPLA_2$ present in articular cartilage [32]. $cPLA_2$ is also reported to be involved in PGE_2 production by osteoblast cells [33], while there are reports indicating that $sPLA_2$ augments $cPLA_2$ expression in mouse osteoblasts via endogenous PGE [13,34]. Because of the significant functional coupling and/or synergism that can exist between $cPLA_2$ and $sPLA_2$ in various cells [3,13,33-35], $sPLA_2$ could conceivably be involved in chondrocyte destruction in RA by playing a role in bone resorption through crosstalk with $cPLA_2$.

We have found significantly elevated levels of circulating $sPLA_2$ in Tg197 mice at 8 weeks of age as compared with the much lower baseline levels detected at 4 weeks of age. Elevated levels of $sPLA_2$ have been reported in the plasma of patients with acute and chronic inflammatory diseases [36]. $sPLA_2$ can mobilize AA to induce the *de novo* synthesis of eicosanoids in a variety of inflammatory cells [37], leading to subsequent release of proinflammatory mediators. Recently, $sPLA_2$ has been shown to amplify TNF-induced PGE_2 synthesis in human rheumatoid synoviocytes [8], a process that is blocked by cyclic peptide inhibitors of human $sPLA_2$ [38]. The use of a low-molecular-weight peptide, such as P-NT.II, that effectively lowers $sPLA_2$ could be of clear clinical benefit in similar situations. Our results obtained with P-NT.II-treated Tg197 mice demonstrated that this new peptide inhibitor significantly suppressed the circulating $sPLA_2$ activity in those mice, whereas scrambled P-NT.II (negative control peptide) was without any effect.

Figure 6

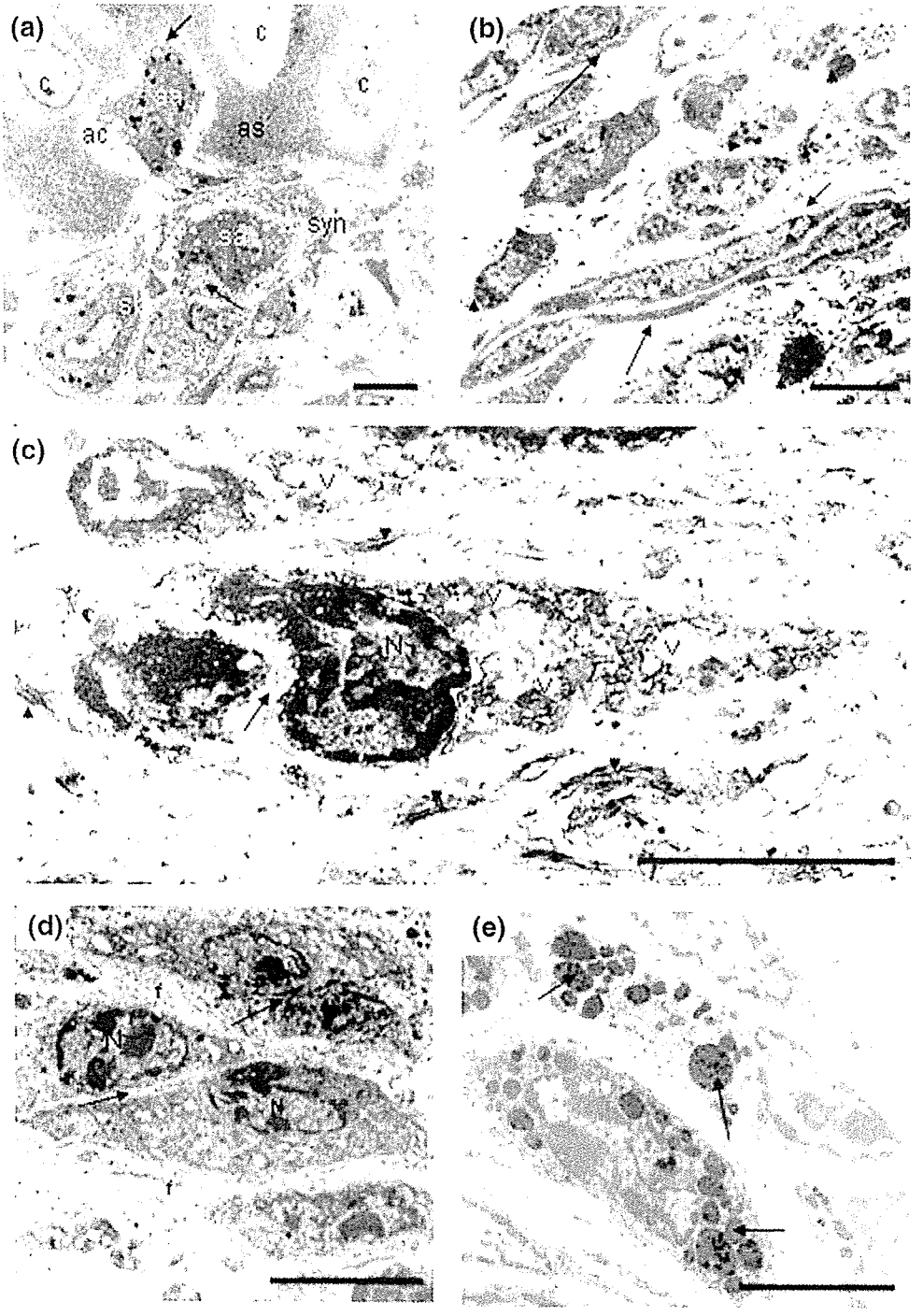

Synovium of untreated Tg197 mice at age 8 weeks. **(a)** Proliferation of the synovial tissue (syn) in the articular cavity (ac) showing macrophage-like type A synoviocytes (sa) with thin cytoplasmic protrusions (arrow) invading the articular surface (as), and closely packed secretory type B synoviocytes (sb) seen in the superficial layer of pannus. **(b)** The synovial membrane was lined by closely packed, elongated (arrow) or rounded synoviocytes with infiltrating cells (arrowhead) present under the synovium. **(c)** Degenerating synoviocyte with disintegrated nuclei (arrow) and vacuolated (v) cytoplasm along with disrupted collagen fibres (arrowhead) randomly seen in the synovium. **(d)** Adherent-type junction (arrow) sealing two synoviocytes with fibrin (f) between them. **(e)** Synoviocytes appeared flattened, and partially degranulated mast cells (arrow) are seen under the synovium. $N = 4$ joints; mean percentage of degenerating synoviocytes = 80% of total cells. Bars = 5 μm. c, chondrocytes; N, nucleus.

Figure 7

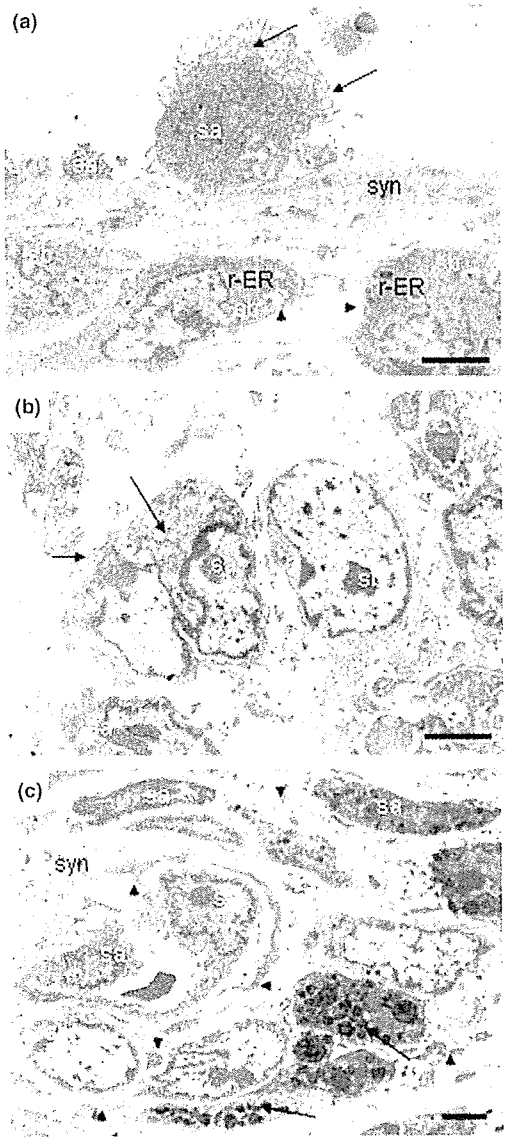

Synovium of treated Tg197 mice. **(a)** Nontransgenic wild-type group (control) at age 8 weeks: type A (sa) and type B (sb) synoviocytes are arranged loosely in the synovium (syn). Type A cells are characterized by many thin filopodia (arrow), while type B cells contain many instances of rough endoplasmic reticulum (r-ER), small vesicles, and basement membrane structures (arrowhead); **(b)** P-NT.II-treated Tg197 group at 5–8 weeks of age: synoviocyte A cells (sa) with characteristic cytoplasmic processes intermingled with those of neighboring cells (arrow) and B cells (sb), seen at age 6–8 weeks of age (i.e. 2–4 weeks post-treatment), appear unmodified during the time course (1–4 weeks) of treatment. The ultrastructural features are similar to those seen in the ankle joints of wild-type controls in (a). **(c)** Scrambled-P-NT.II-treated Tg197 group at age 8 weeks: type A (sa) and B (sb) synovial cells were seen lining up close together, and many cell fragments (arrowheads) resulting from fibrous degeneration of endothelial cells were present in the synovium (syn), along with infiltrating mast cells (arrows). $N = 4$ joints/group; mean percentage of degenerating synoviocytes = 24% and 75% of total in (b) and (c), respectively. Bars = 2 μm.

Figure 8

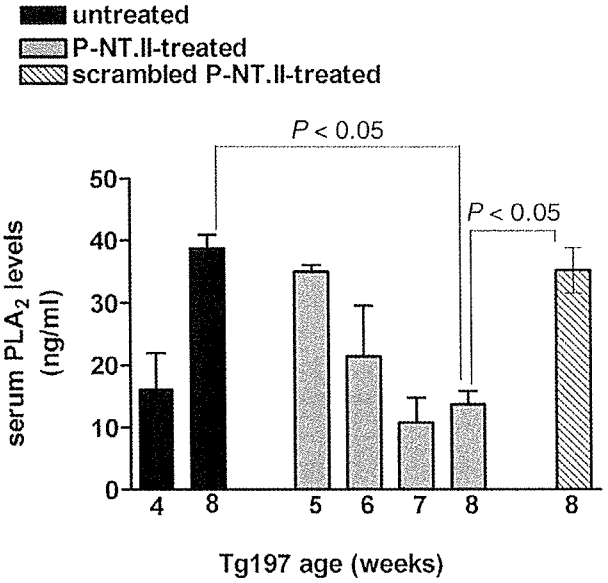

Time course of serum phospholipase A_2 ($sPLA_2$) levels. Serum $sPLA_2$ levels were measured with an *Escherichia coli* membrane assay in blood samples collected from untreated, P-NT.II-treated, and scrambled-P-NT.II-treated Tg197 mice at weekly intervals during the 4 weeks' time course of treatment. Values are the mean ± SD ($N = 4$/group). One-way ANOVA with Bonferroni's multiple comparison post test: $P < 0.05$, untreated versus P-NT.II-treated (age 8 weeks); $P < 0.05$, scrambled-P-NT.II-treated versus P-NT.II-treated (age 8 weeks).

The data obtained from the present study suggest that P-NT.II ameliorates synovitis and bone and cartilage erosions in the joints through modulation of circulatory and localized $sPLA_2$, which might otherwise amplify TNF-dependent pathways in rheumatoid synovium. Although the mode of action of $sPLA_2$ in this animal model is not exactly known, the potential mechanism may involve binding to a receptor [39], followed by internalization [40] and transfer of $sPLA_2$ to intracellular pools of phospholipids enriched in AA [41]. Further catalysis by $sPLA_2$ through surface interactions can then initiate and promote pathology by releasing AA, which can subsequently be converted to proinflammatory prostaglandins and leukotrienes. There are no published reports of $sPLA_2$ inhibitors showing benefit on bone erosion. The ultrastructural evidence of the beneficial effect of the peptide on joint destruction as shown here suggests a possible use of $sPLA_2$ inhibitors in the treatment of inflammatory bone loss diseases such as RA. However, some caution is advisable in the interpretation of the findings, since the nature of the arthritis in a purely TNF-driven disease, such as that observed in TNF transgenic mice, may not truly reflect the situation in human inflammatory joint diseases.

Conclusion

The present study provides ultrastructural demonstration of the modulatory effect of the P-NT.II peptide on synovial

Figure 9

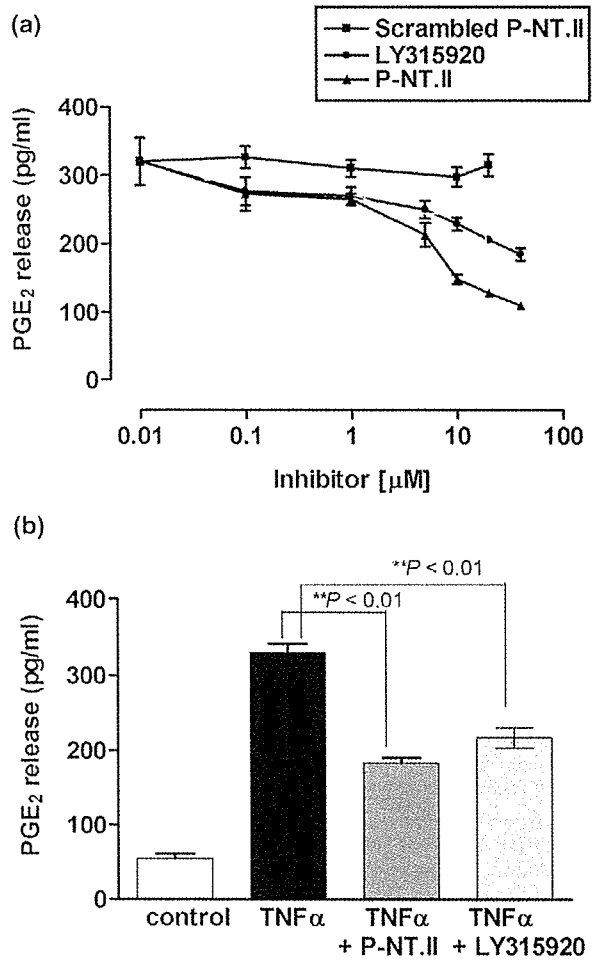

Modulation of lipopolysaccharide (LPS)- and tumor necrosis factor (TNF)-stimulated PGE_2 release. Macrophages (5×10^5 cells/ml) from subcultured J774 mouse cell line were incubated with **(a)** LPS (2 μg/ml) or **(b)** TNF (10 ng/ml) in the absence or the presence of various concentrations (0–40 μM) of P-NT.II, LY315920, or scrambled P-NT.II for 20 hours. Supernatants were collected, and PGE_2 release in the medium was determined by enzyme-linked immunosorbent assay. Results are shown as the mean ± SEM of five experiments performed in duplicate. $^{**}P < 0.01$ between inhibitor-treated and untreated cultures.

inflammation and joint destruction in TNF-driven Tg197 mouse model of human RA. The results suggest that $sPLA_2$ seems to play a significant role in inflammatory arthritis, and $sPLA_2$ inhibitors may be useful for the development of novel agents to treat RA and other inflammatory diseases.

Competing interests

None declared.

Acknowledgements

We are grateful to Mr Spiros Lalos and Ms Alexia Giannakopoulou, Institute of Immunology, Biomedical Sciences Research Centre, Al Fleming, Greece, and Ms Ng Geok Lan and Ms Chan Yee Gek, Department of Anatomy, Faculty of Medicine, National University of Singapore, for their excellent technical assistance.

References

1. Nevalainen TJ, Haapamaki MM, Gronroos JM: **Roles of secretory phospholipases A(2) in inflammatory diseases and trauma.** *Biochim Biophys Acta* 2000, **1488**:83-90.
2. Lin MK, Farewell V, Vadas P, Bookman AA, Keystone EC, Pruzanski W: **Secretory phospholipase A2 as an index of disease activity in rheumatoid arthritis. Prospective double blind study of 212 patients.** *J Rheumatol* 1996, **23**:1162-1166.
3. Huwiler A, Staudt G, Kramer RM, Pfeilschifter J: **Cross-talk between secretory phospholipase A2 and cytosolic phospholipase A2 in rat renal mesangial cells.** *Biochim Biophys Acta* 1997, **1348**:257-272.
4. Jamal OS, Conaghan PG, Cunningham AM, Brooks PM, Munro VF, Scott KF: **Increased expression of human type IIa secretory phospholipase A2 antigen in arthritic synovium.** *Ann Rheum Dis* 1998, **57**:550-558.
5. Vadas P, Pruzanski W, Kim J, Fox N: **The proinflammatory effect of intra-articular injection of soluble human and venom phospholipase A2.** *Am J Pathol* 1989, **134**:807-811.
6. Bomalaski JS, Lawton P, Browning JL: **Human extracellular recombinant phospholipase A2 induces an inflammatory response in rabbit joints.** *J Immunol* 1991, **146**:3904-3910.
7. Lin MK, Katz A, van den BH, Kennedy B, Stefanski E, Vadas P, Pruzanski W: **Induction of secretory phospholipase A2 confirms the systemic inflammatory nature of adjuvant arthritis.** *Inflammation* 1998, **22**:161-173.
8. Bidgood MJ, Jamal OS, Cunningham AM, Brooks PM, Scott KF: **Type IIA secretory phospholipase A2 up-regulates cyclooxygenase-2 and amplifies cytokine-mediated prostaglandin production in human rheumatoid synoviocytes.** *J Immunol* 2000, **165**:2790-2797.
9. Feldmann M: **What is the mechanism of action of anti-tumour necrosis factor-alpha antibody in rheumatoid arthritis?** *Int Arch Allergy Immunol* 1996, **111**:362-365.
10. Akira S, Kishimoto T: **IL-6 and NF-IL6 in acute-phase response and viral infection.** *Immunol Rev* 1992, **127**:25-50.
11. Papadakis KA, Targan SR: **Tumor necrosis factor: biology and therapeutic inhibitors.** *Gastroenterology* 2000, **119**:1148-1157.
12. Triggiani M, Granata F, Oriente A, Gentile M, Petraroli A, Balestrieri B, Marone G: **Secretory phospholipases A2 induce cytokine release from blood and synovial fluid monocytes.** *Eur J Immunol* 2002, **32**:67-76.
13. Murakami M, Kuwata H, Amakasu Y, Shimbara S, Nakatani Y, Atsumi G, Kudo I: **Prostaglandin E2 amplifies cytosolic phospholipase A2- and cyclooxygenase-2-dependent delayed prostaglandin E2 generation in mouse osteoblastic cells. Enhancement by secretory phospholipase A2.** *J Biol Chem* 1997, **272**:19891-19897.
14. Schrier DJ, Flory CM, Finkel M, Kuchera SL, Lesch ME, Jacobson PB: **The effects of the phospholipase A2 inhibitor, manoalide, on cartilage degradation, stromelysin expression, and synovial fluid cell count induced by intraarticular injection of human recombinant interleukin-1 alpha in the rabbit.** *Arthritis Rheum* 1996, **39**:1292-1299.
15. Garcia-Pastor P, Randazzo A, Gomez-Paloma L, Alcaraz MJ, Paya M: **Effects of petrosaspongiolide M, a novel phospholipase A2 inhibitor, on acute and chronic inflammation.** *J Pharmacol Exp Ther* 1999, **289**:166-172.
16. Miele L: **Antiflammins. Bioactive peptides derived from uteroglobin.** *Ann N Y Acad Sci* 2000, **923**:128-140.
17. Thwin MM, Gopalakrishnakone P, Kini RM, Armugam A, Jeyaseelan K: **Recombinant antitoxic and antiinflammatory factor from the nonvenomous snake Python reticulatus: phospholipase A2 inhibition and venom neutralizing potential.** *Biochemistry* 2000, **39**:9604-9611.
18. Thwin MM, Satish RL, Chan ST, Gopalakrishnakone P: **Functional site of endogenous phospholipase A2 inhibitor from python serum.** *Eur J Biochem* 2002, **269**:719-727.
19. Thwin MM, Ong WY, Fong CW, Sato K, Kodama K, Farooqui AA, Gopalakrishnakone P: **Secretory phospholipase A2 activity in the normal and kainate injected rat brain, and inhibition by a**

peptide derived from python serum. *Exp Brain Res* 2003, **150:**427-433.
20. Keffer J, Probert L, Cazlaris H, Georgopoulos S, Kaslaris E, Kioussis D, Kollias G: **Transgenic mice expressing human tumour necrosis factor: a predictive genetic model of arthritis.** *EMBO J* 1991, **10:**4025-4031.
21. Wooley PH: **Collagen-induced arthritis in the mouse.** *Methods Enzymol* 1988, **162:**361-373.
22. Douni E, Sfikakis PP, Haralambous S, Fernandes P, Kollias G: **Attenuation of inflammatory polyarthritis in TNF transgenic mice by diacerein: comparative analysis with dexamethasone, methotrexate and anti-TNF protocols.** *Arthritis Res Ther* 2004, **6:**R65-R72.
23. Arsenault AL, Lhotak S, Hunter WL, Banquerigo ML, Brahn E: **Taxol (paclitaxel) involution of articular cartilage destruction in collagen induced arthritis: an ultrastructural demonstration of an increased superficial chondroprotective layer.** *J Rheumatol* 2000, **27:**582-588.
24. Henzgen S, Petrow PK, Thoss K, Brauer R: **Degradation of articular cartilage during the progression of antigen-induced arthritis in mice. A scanning and transmission electron microscopic study.** *Exp Toxicol Pathol* 1996, **48:**255-263.
25. Lapadula G, Nico B, Cantatore FP, La Canna R, Roncali L, Pipitone V: **Early ultrastructural changes of articular cartilage and synovial membrane in experimental vitamin A-induced osteoarthritis.** *J Rheumatol* 1995, **22:**1913-1921.
26. Ghadially FN: *Fine structure of the synovial joints. A text and atlas of the ultrastructure of normal and pathological articular tissues* London: Butterworth; 1983.
27. Redlich K, Hayer S, Maier A, Dunstan CR, Tohidast-Akrad M, Lang S, Turk B, Pietschmann P, Woloszczuk W, Haralambous S, Kollias G, Steiner G, Smolen JS, Schett G: **Tumor necrosis factor alpha-mediated joint destruction is inhibited by targeting osteoclasts with osteoprotegerin.** *Arthritis Rheum* 2002, **46:**785-792.
28. Han Z, Chang L, Yamanishi Y, Karin M, Firestein GS: **Joint damage and inflammation in c-Jun N-terminal kinase 2 knockout mice with passive murine collagen-induced arthritis.** *Arthritis Rheum* 2002, **46:**818-823.
29. Snyder DW, Bach NJ, Dillard RD, Draheim SE, Carlson DG, Fox N, Roehm NW, Armstrong CT, Chang CH, Hartley LW, Johnson LM, Roman CR, Smith AC, Song M, Fleisch JH: **Pharmacology of LY315920/S-5920, [[3-(aminooxoacetyl)-2-ethyl-1- (phenylmethyl)-1H-indol-4-yl]oxy] acetate, a potent and selective secretory phospholipase A2 inhibitor: A new class of anti-inflammatory drugs, SPI.** *J Pharmacol Exp Ther* 1999, **288:**1117-1124.
30. Li P, Schwarz EM: **The TNF-alpha transgenic mouse model of inflammatory arthritis.** *Springer Semin Immunopathol* 2003, **25:**19-33.
31. Nevalainen TJ, Marki F, Kortesuo PT, Grutter MG, Di Marco S, Schmitz A: **Synovial type (group II) phospholipase A2 in cartilage.** *J Rheumatol* 1993, **20:**325-330.
32. Pruzanski W, Bogoch E, Katz A, Wloch M, Stefanski E, Grouix B, Sakotic G, Vadas P: **Induction of release of secretory nonpancreatic phospholipase A2 from human articular chondrocytes.** *J Rheumatol* 1995, **22:**2114-2119.
33. Miyaura C, Inada M, Matsumoto C, Ohshiba T, Uozumi N, Shimizu T, Ito A: **An essential role of cytosolic phospholipase A2alpha in prostaglandin E2-mediated bone resorption associated with inflammation.** *J Exp Med* 2003, **197:**1303-1310.
34. Kudo I, Murakami M: **Diverse functional coupling of prostanoid biosynthetic enzymes in various cell types.** *Adv Exp Med Biol* 1999, **469:**29-35.
35. Balsinde J, Balboa MA, Insel PA, Dennis EA: **Regulation and inhibition of phospholipase A2.** *Annu Rev Pharmacol Toxicol* 1999, **39:**175-189.
36. Vadas P: **Elevated plasma phospholipase A2 levels: correlation with the hemodynamic and pulmonary changes in gram-negative septic shock.** *J Lab Clin Med* 1984, **104:**873-881.
37. Mayer RJ, Marshall LA: **New insights on mammalian phospholipase A2(s); comparison of arachidonoyl-selective and -nonselective enzymes.** *FASEB J* 1993, **7:**339-348.
38. Church WB, Inglis AS, Tseng A, Duell R, Lei PW, Bryant KJ, Scott KF: **A novel approach to the design of inhibitors of human secreted phospholipase A2 based on native peptide inhibition.** *J Biol Chem* 2001, **276:**33156-33164.
39. Lambeau G, Lazdunski M: **Receptors for a growing family of secreted phospholipases A2.** *Trends Pharmacol Sci* 1999, **20:**162-170.
40. Murakami M, Koduri RS, Enomoto A, Shimbara S, Seki M, Yoshihara K, Singer A, Valentin E, Ghomashchi F, Lambeau G, Gelb MH, Kudo I: **Distinct arachidonate-releasing functions of mammalian secreted phospholipase A2s in human embryonic kidney 293 and rat mastocytoma RBL-2H3 cells through heparan sulfate shuttling and external plasma membrane mechanisms.** *J Biol Chem* 2001, **276:**10083-10096.
41. Granata F, Balestrieri B, Petraroli A, Giannattasio G, Marone G, Triggiani M: **Secretory phospholipases A2 as multivalent mediators of inflammatory and allergic disorders.** *Int Arch Allergy Immunol* 2003, **131:**153-163.

Chemistry & Biology, Vol. 11, 1053–1058, August, 2004, ©2004 Elsevier Ltd. All rights reserved. · DOI 10.1016/j.chembiol.2004.05.012

Modification of Intracellular Ca^{2+} Dynamics by Laser Inactivation of Inositol 1,4,5-Trisphosphate Receptor Using Membrane-Permeant Probes

Takatoshi Yogo,[1] Kazuya Kikuchi,[1,3] Takanari Inoue,[1] Kenzo Hirose,[2] Masamitsu Iino,[2] and Tetsuo Nagano[1,*]
[1]Graduate School of Pharmaceutical Sciences
[2]Department of Pharmacology
Graduate School of Medicine
The University of Tokyo
7-3-1 Hongo
Bunkyo-ku, Tokyo 113-0033
[3]PRESTO
Japan Science and Technology Corporation
Kawaguchi, Saitama
Japan

Summary

A membrane-permeant malachite green-conjugated IP_3 analog ($MGIP_3$/PM) was synthesized as a probe for small molecule-based CALI (smCALI), and its effect on the Ca^{2+} signaling in intact DT40 chicken B cells was examined. In DT40 B cells treated with the smCALI probe, laser irradiation inhibited IP_3-induced Ca^{2+} oscillations in response to B cell receptor stimulation, demonstrating that IP_3R was acutely inactivated. We then applied smCALI to clarify the mechanism of capacitative Ca^{2+} entry (CCE), in which involvement of IP_3R has been suggested. Despite the inactivation of IP_3R by smCALI, thapsigargin-induced CCE remained unaffected, providing evidence that functional IP_3R is not required for CCE in DT40 cells. These results demonstrate the potency of the smCALI technique for the study of the roles of IP_3R in complex intracellular Ca^{2+} dynamics.

Introduction

Specific inactivation of biomolecules has been one of the most widely used approaches to study the physiological functions of these molecules, and various methods, including the use of pharmacological antagonists, targeted gene disruption, and antibodies, have been used. The activities of most functional biomolecules depend upon the site of expression and the nature of the cellular processes in which they are involved [1–3], so a technique for inactivation of target proteins in a spatiotemporally well controlled manner should be extremely useful. To achieve this purpose, chromophore-assisted laser inactivation (CALI) is an excellent method [4, 5], in which the protein of interest is targeted by an exogenously introduced antibody that has been tagged with a CALI chromophore, usually malachite green, and the chromophore-antibody complex is subsequently irradiated with intense localized laser light. The irradiated chromophore produces radical species that react with the protein to which the antibody is bound, causing its inactivation. Because the radical species are highly reactive and have very short lifetimes, the antibody-recognized proteins are specifically inactivated. The functions of various molecules, which could not have been analyzed by other currently available methods, have been elucidated by inactivation of target proteins at the appropriate site and time using the CALI technique.

Although CALI has proved very powerful, it has some limitations, which are primarily attributable to the use of antibody for the molecular recognition. It is difficult to label antibodies with chromophores at specific amino acid residues, so that the extent of the damage inflicted on the target protein cannot readily be controlled. Moreover, it is necessary to use an invasive method to introduce antibodies into cells, which may jeopardize the physiological functions and long-term viability of the cells. Further, invasive methods (such as trituration, whole-cell clamp, or microinjection) can be applied to only a few cells at a time and are not applicable to tissues.

To circumvent the limitations associated with conventional CALI, we have set out to develop a new method in which synthetic small molecules are used instead of antibody for target recognition (small molecule-based CALI, or smCALI). We designed and synthesized suitable synthetic small molecular probes for biological application of CALI. For the implementation of smCALI, we chose inositol 1,4,5-trisphosphate receptor (IP_3R) as a target protein. IP_3R is a Ca^{2+} channel localized on the endoplasmic reticulum (ER) membrane, and regulates the cytosolic Ca^{2+} concentration, playing an important role in various physiological functions, such as contraction, secretion, fertilization, synaptic plasticity, and gene expression [6, 7]. Thus, spatiotemporally controlled inactivation of IP_3R using smCALI should be useful for studying of the role of the protein in these functions.

We developed a chromophore-labeled IP_3 analog (carboxymalachite green-aminopropyl-1D-*myo*-inositol-1,4,5-trisphosphate, $MGIP_3$) and showed that spatially controlled inactivation of IP_3R could be achieved within a few seconds by $MGIP_3$-mediated smCALI [8–10]. The time required for smCALI is very much shorter than that of antibody-based CALI, which usually requires ~5 min. Furthermore, by focusing a laser beam at the subcellular level in a single PC12 cell, precise control of the area of inactivation could be achieved. In the present study, we derivatized $MGIP_3$ to a membrane-permeant compound for noninvasive delivery into living cells. This membrane-permeant probe can be easily applied to intact cells or cell populations and smCALI experiments can be conducted under physiological conditions. We describe here the successful application of smCALI in intact cells using the membrane-permeant probe, and we show that smCALI provides a powerful tool to analyze complex intracellular Ca^{2+} dynamics.

Results and Discussion

$MGIP_3$/PM Permeates through the Plasma Membrane and Interacts with IP_3R

In previous studies, we designed and synthesized a chromophore-labeled IP_3 analog ($MGIP_3$, Figure 1) and

*Correspondence: tlong@mol.f.u-tokyo.ac.jp

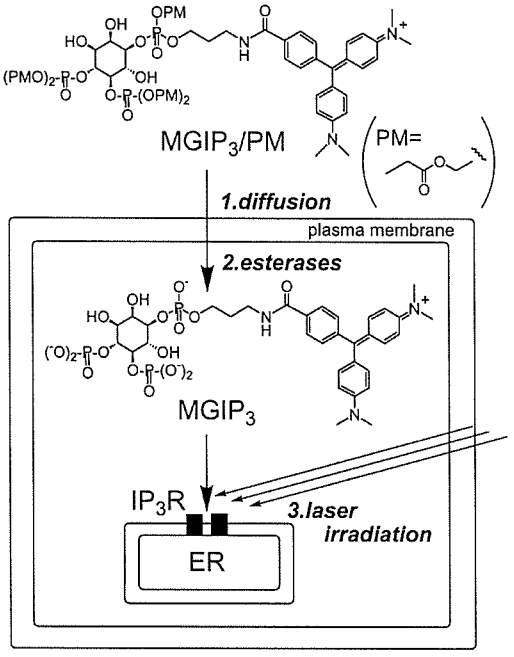

Figure 1. Scheme of smCALI Using a Membrane-Permeant Synthetic Probe, $MGIP_3/PM$

IP_3R, inositol 1,4,5-trisphosphate receptor; ER, endoplasmic reticulum; PM, propionyloxymethyl group.

showed that $MGIP_3$ could act as an agonist of IP_3R and function as an effective probe for smCALI of IP_3R [9, 10]. Permeabilization of the cell membrane or whole-cell patch-clamp was required to introduce $MGIP_3$ into cells, because $MGIP_3$ cannot permeate through the plasma membrane due to its charge and hydrophilicity. Thus, we derivatized $MGIP_3$ to a membrane-permeant compound (carboxymalachite green-aminopropyl-1D-*myo*-inositol-1,4,5-trisphosphate hexakis (propionyloxymethyl) ester, $MGIP_3/PM$, Figure 1) by masking all the anionic phosphate groups with propionyloxymethyl esters. This compound is expected to diffuse into cells, where it should undergo cleavage by the ubiquitous intracellular esterases to generate the hydrolyzed form (i.e., $MGIP_3$), which binds to IP_3R (Figure 1).

We examined whether $MGIP_3/PM$ can indeed permeate through the plasma membrane and interact with IP_3R by using DT40 cells expressing type 2 IP_3R (IP_3R-2). $MGIP_3$ is an agonist of IP_3R and induces Ca^{2+} release via IP_3R in permeablized DT40 cells. Thus, one would expect to observe an increase in $[Ca^{2+}]_i$, if extracellularly applied $MGIP_3/PM$ dose permeate through the plasma membrane and subsequently undergo hydrolysis to yield $MGIP_3$. When $MGIP_3/PM$ (100 μM) was added to the extracellular solution of DT40 cells, it induced an increase in $[Ca^{2+}]_i$, indicating that $MGIP_3/PM$ did enter the cells and interact with IP_3R (Figure 2A, black trace; Figure 2B). On the other hand, extracellularly added $MGIP_3$ (100 μM) or vehicle (0.1% DMSO) induced no detectable $[Ca^{2+}]_i$ increase (Figure 2A, green and blue

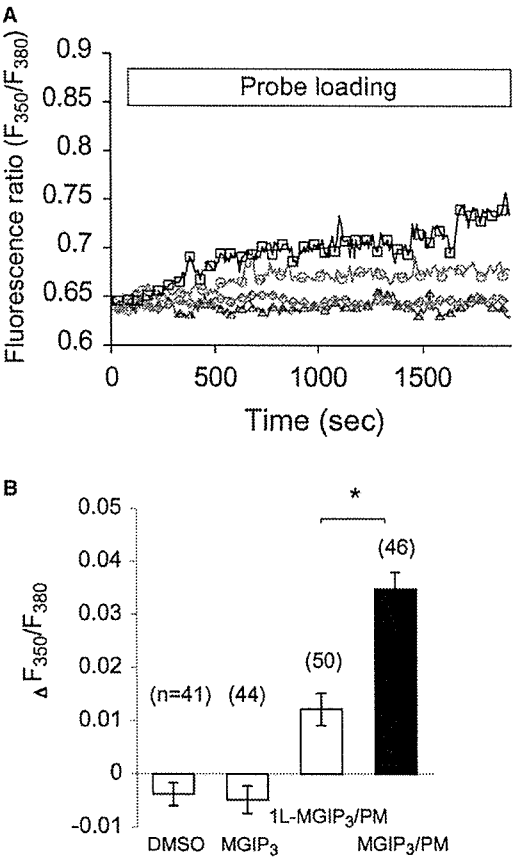

Figure 2. $[Ca^{2+}]_i$ Increase Induced by 100 μM $MGIP_3/PM$ in Intact DT40 Cells

(A) $[Ca^{2+}]_i$ increase induced by 100 μM $MGIP_3/PM$, 100 μM 1L-$MGIP_3/PM$, 100 μM $MGIP_3$, and vehicle (0.1% DMSO). Test compounds were added to an extracellular solution of Fura-2-loaded DT40 cells as indicated by the box. All traces show Ca^{2+} responses in single DT40 cells. 100 μM $MGIP_3/PM$ (black square) induced a much greater $[Ca^{2+}]_i$ increase than 100 μM 1L-$MGIP_3/PM$ (red circle). 100 μM $MGIP_3$ (green diamond) or vehicle (blue triangle) induced no detectable $[Ca^{2+}]_i$ increase.

(B) $[Ca^{2+}]_i$ increase induced by 100 μM $MGIP_3/PM$ and 100 μM 1L-$MGIP_3/PM$. 100 μM $MGIP_3/PM$ induced a significantly larger increase of the fluorescence ratio than 100 μM 1L-$MGIP_3/PM$ within 1800 s after extracellular addition of each compound (*$p < 0.0001$). These data were acquired in two independent experiments. The number of analyzed cells is indicated on top of each column. Results are the mean ± SEM.

traces; Figure 2B), indicating that masking of the phosphate groups is essential for membrane permeation. As a control experiment, we used the optical isomer of $MGIP_3/PM$ (1L-$MGIP_3/PM$), which has the same photochemical nature as that of $MGIP_3/PM$, though its hydrolyzed form (i.e., 1L-$MGIP_3$) has a much weaker agonistic effect on IP_3R [9, 10]. 1L-$MGIP_3/PM$ (100 μM) was much less effective in increasing $[Ca^{2+}]_i$ than $MGIP_3/PM$ and a significant difference in their Ca^{2+} releasing activity was observed (Figures 2A, red versus black traces; Figure 2B, $p < 0.0001$). In all experiments, cells

showed the same responses to B cell receptor stimulation. We also examined the concentration of $MGIP_3$ in the cell by HPLC. After uptake of $MGIP_3$/PM from the exracellular solution by DT40 cells, cells were washed and disrupted by sonication; then the intracellular solution was analyzed by HPLC. The result suggested that the concentration of $MGIP_3$ was at most 10 μM in the cell when $MGIP_3$/PM was extracellularly applied at a concentration of 100 μM (data not shown). This range of $MGIP_3$ concentration is the same as that used in the previous study [10], in which the specificity of CALI was established. Furthermore, DT40 cells lacking all three type of IP_3R [11] exhibited no detectable $[Ca^{2+}]_i$ increase in response to extracellular addition of 100 μM $MGIP_3$/PM (data not shown). These results indicate that $MGIP_3$/PM can permeate through the plasma membrane and interact with IP_3R after intracellular hydrolysis.

Although $MGIP_3$/PM has an inherent agonistic effect, at low concentrations $MGIP_3$/PM induced no detectable $[Ca^{2+}]_i$ increase. Indeed, there was no significant difference between the increase of fluorescence ratio induced by 4 μM $MGIP_3$/PM and that by 4 μM 1L-$MGIP_3$/PM (-0.009 ± 0.006 and -0.013 ± 0.006, respectively, $p = 0.6825$). Thus, we used 4 μM $MGIP_3$/PM for smCALI so that the agonistic effect of the ester could be neglected.

$MGIP_3$/PM-Mediated smCALI Inactivates IP_3R in Intact DT40 Cells

Stimulating the B cell antigen receptor (BCR) induces production of IP_3 via phospholipase C (PLC)-γ2, followed by repetitive cyclic increases in $[Ca^{2+}]_i$ (Ca^{2+} oscillation) in DT40 cells [12]. In the previous study, we showed that $MGIP_3$-mediated smCALI inhibited IP_3-induced Ca^2 release in permeabilized DT40 cells [10]. We then examined whether laser beam irradiation focused onto intact single DT40 cells loaded with $MGIP_3$/PM induces protein inactivation, by measuring the IP_3-induced Ca^{2+} oscillation. Fura-2-loaded DT40 cells were loaded with 4 μM $MGIP_3$/PM for 60 min, and then we routinely allowed an incubation period of $\geq$30 min to ensure complete hydrolysis of $MGIP_3$/PM after wash-out of excess ester. $MGIP_3$ in the cell is expected to be stable because it has been shown that inositol 1,4,5- trisphosphate derivatives modified at 1-phosphate are not substrates for 5-phosphatase or 3-kinase [13]. Subsequently, several $MGIP_3$/PM-loaded cells were successively irradiated with the laser for 60 s each (Figure 3A), followed by induction of Ca^{2+} oscillation by BCR stimulation with anti-BCR antibody M4 (1 μg ml^{-1}) [12]. Ca^{2+} oscillation was strongly inhibited in irradiated cells (Figure 3B). The average number of Ca^{2+} oscillations within 500 s after BCR stimulation was decreased by 50% in irradiated cells compared with nonirradiated cells (Figures 3C and 3D, $p < 0.0001$). $MGIP_3$/PM-mediated smCALI also decreased the average peak amplitude of Ca^{2+} oscillations: 2.04 ± 0.10 in irradiated cells and 2.41 ± 0.07 in nonirradiated cells ($p < 0.005$).

Laser irradiation alone in the absence of $MGIP_3$/PM had no significant effect on the average number of Ca^{2+} oscillations (Figure 3D, $p > 0.82$). We then examined whether or not the laser-induced inhibitory effect on Ca^{2+} oscillation is also observed in 1L-$MGIP_3$/PM-loaded cells. No effect of laser irradiation on the average number of Ca^{2+} oscillations was observed in cells loaded with 4 μM 1L-$MGIP_3$/PM (Figure 3D, $p > 0.36$). These results indicate that there is no nonspecific laser damage to IP_3R, and that the inhibition of Ca^{2+} oscillation was the result of IP_3R inactivation by $MGIP_3$/PM-mediated smCALI.

$MGIP_3$-mediated smCALI has been shown to inhibit IP_3-induced Ca^{2+} release [10]. Therefore, it seems likely that Ca^{2+} oscillation was inhibited as a result of the inhibition of IP_3-induced Ca^{2+} release. Ca^{2+} oscillation is a genuine physiological phenomenon, and it is not appropriate to analyze it by using methods that disrupt the intact cell structure, for example, using detergents or microinjection. SmCALI provides the opportunity to analyze Ca^{2+} signaling under physiological conditions.

It was not clear quantitatively to what extent the IP_3R was inactivated by our procedure, but the oscillation frequency, an important factor of Ca^{2+} signaling, was greatly reduced, except for a few initial spikes, as a result of IP_3R inactivation.

Absence of Involvement of IP_3R in Capacitative Calcium Entry

After release of Ca^{2+} from intracellular stores via IP_3R, Ca^{2+} entry across the plasma membrane follows in many cell types [14]. This Ca^{2+} signaling is called capacitative Ca^{2+} entry (CCE). CCE is thought to form an important component of Ca^{2+} signaling. Although IP_3R has been implicated in CCE, the molecular mechanism of CCE remains elusive [15–17]. To study whether IP_3R is involved in CCE, CCE was examined in cells in which IP_3R had been inactivated by smCALI. Inactivation of IP_3R in DT40 cells expressing IP_3R-2 by smCALI was carried under the same conditions as the above experiments. Ca^{2+} stores were then depleted by applying 1 μM thapsigargin (TG), an inhibitor of sarco/endoplasmic reticulum Ca^{2+}-ATPase (SERCA) [18], in the absence of extracellular Ca^{2+}. Subsequent addition of 2 mM Ca^{2+} evoked an increase in $[Ca^{2+}]_i$ due to CCE (Figure 4A). The amplitude of the CCE-mediated increase in $[Ca^{2+}]_i$ was not significantly different between irradiated and nonirradiated cells ($p > 0.86$, Figure 4B), suggesting that the activation of IP_3R is not essential for TG-induced CCE in DT40 cells under these experimental conditions.

It has been suggested that CCE is regulated by the IP_3R [15]. However, it has been difficult to acutely and specifically inactivate IP_3R. Most of the conventional antagonists of IP_3R have direct inhibitory effects on CCE [17, 19]. Targeted disruption of the IP_3R genes is a powerful method, but may not be free from possible long-term compensatory reactions. Recent findings using mutant DT40 cells, in which all subtypes of IP_3R were deleted, strongly suggested that IP_3R is not involved in CCE, because the cells showed typical CCE or I_{crac} (calcium release-activated calcium current) identical to that observed in wild-type cells [11, 16, 20, 21]. However, it was suggested that ryanodine receptors would work as a compensatory mechanism in the mutant DT40 cells [22]. Taking the above circumstances into consideration, smCALI appears to be an excellent method to analyze the functions of IP_3R in CCEs, because acute

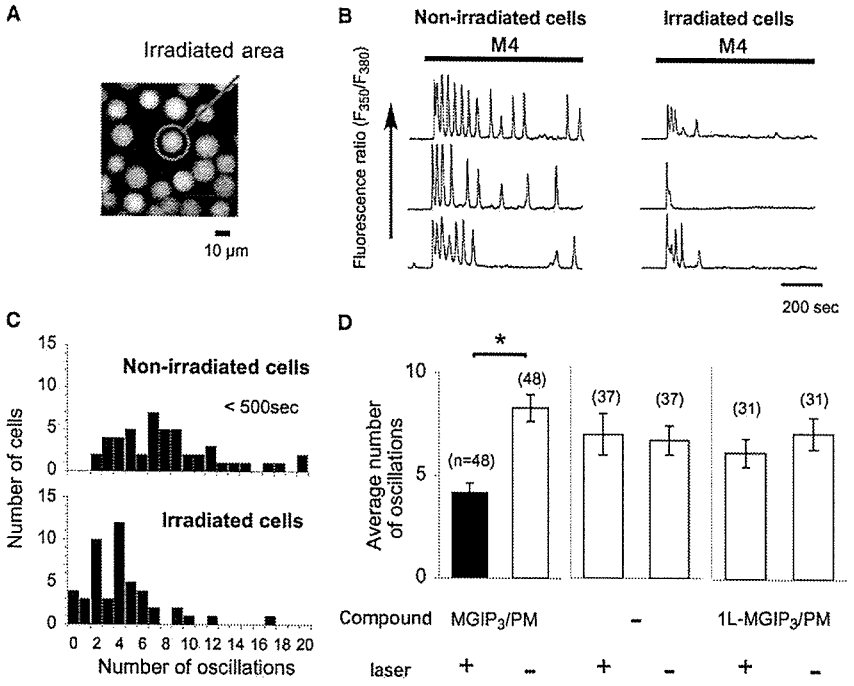

Figure 3. Inhibitory Effect of MGIP$_3$/PM-Mediated smCALI on Ca^{2+} Oscillations in Intact DT40 Cells

(A) Fluorescence image of DT40 cells excited at 350 nm after loading Fura-2AM. The red circle indicates the laser spot for irradiation.

(B) Ca^{2+} responses upon ligation of BCR with anti-BCR antibody (1 μg ml^{-1}) after smCALI with 4 μM MGIP$_3$/PM. Traces show several representative responses in irradiated or nonirradiated cells. Antibody was applied as indicated by horizontal bars above the traces.

(C) Histogram showing the number of Ca^{2+} oscillations within 500 s of BCR stimulation in irradiated or nonirradiated cells (48 cells in each condition).

(D) Average number of Ca^{2+} oscillations in response to BCR stimulation after the indicated treatment. A significant difference was found between the average numbers of Ca^{2+} oscillations under irradiated and nonirradiated conditions with MGIP$_3$/PM (*$p < 0.0001$). The number of analyzed cells is indicated on top of each column. These data were acquired in six independent experiments. Results are the mean ± SEM.

inactivation of IP$_3$R can be carried out under physiological conditions. Other studies have also shown that acute inhibition of IP$_3$R by heparin (a potent IP$_3$R angagonist) failed to inhibit I_{crac} [20, 21, 23]. Our results provided evidence that IP$_3$R is not involved in CCE in DT40 cells. Further application of smCALI should clarify the function of IP$_3$R in CCE in other cell types.

In the present study we showed that smCALI can overcome the main limitation of the conventional CALI technique, in which invasive methods have to be used to introduce antibodies into cells. Indeed, we have succeeded in examining the effect of smCALI on Ca^{2+} oscillations. The role of IP$_3$R in CCE could be analyzed by smCALI without any long-term compensatory effect. Spatiotemporally controlled genetic modification (conditional knockout) [24] has emerged as a powerful molecular inactivation method. However, it requires a much longer time for molecular inactivation than smCALI. Thus, smCALI provides a unique method to analyze Ca^{2+} signaling under physiological conditions in various cell types. Another feature of MGIP$_3$-mediated smCALI is the catalytic inactivation mechanism [10], i.e., the small-molecular probe (MGIP$_3$) may rapidly associate with and rapidly dissociate from its target (IP$_3$Rs), and repetitive excitation of malachite green causes cumulative inactivation of IP$_3$Rs. Due to the catalytic nature of the inactivation, even a low probe concentration may cause sufficient inactivation. Indeed, we showed that 4 μM MGIP$_3$/PM caused sufficient inactivation of IP$_3$Rs without any agonistic effect. Thus, the smCALI technique provides high spatiotemporal resolution in molecular inactivation, and should be applicable to studies of various physiological functions, especially in polarized cells such as neurons.

Significance

Biological application of conventional CALI has been hampered mainly by the necessity to use invasive methods to introduce antibodies into the cells for target recognition. In the present study, we successfully carried out smCALI in intact cells by using membrane-permeant synthetic small molecules. Some variations of small molecule-based CALI have been developed. For example, arsenic chromophore derivatives designed to specifically bind to a tetracysteine tag attached to a target protein induce target inactivation under light illumination (FlAsH-FALI) [25, 26]. Although